Intrinsic states and collective structures in ^{180}Ta

G. D. Dracoulis, S. M. Mullins, A. P. Byrne, F. G. Kondev, T. Kibédi, S. Bayer, G. J. Lane, T. R. McGoram, and P. M. Davidson
Department of Nuclear Physics, RSPhysSE, Australian National University, Canberra ACT, 0200, Australia
(Received 7 April 1998)

Excited states in ^{180}Ta have been identified using the ^{176}Yb(^{11}B,$\alpha 3n$)^{180}Ta and ^{176}Yb(^{7}Li,$3n$)^{180}Ta reactions and associated time-correlated γ-ray spectroscopy, including particle-γ coincidences for channel selection. As well as identifying the rotational band based on the 9^- two-quasiparticle state at 75 keV, at least eight other low-lying two-quasiparticle states and associated rotational bands have been established. Lifetimes in the few nanosecond region were isolated using γ-γ-time techniques. Most of the observed two-quasiparticle states and some of the band members can be identified with states known from particle transfer studies. The properties of the observed $\Omega_n \pm \Omega_p$ partners of 1^+ and 8^+ bands from the $\nu 9/2^+[624] \otimes \pi 7/2^+[404]$ configuration and the 0^- and 9^- pair from the $\nu 9/2^+[624] \otimes \pi 9/2^-[514]$ configuration are discussed. High-K structures identified include the band based on the four-quasiparticle 45 μs, 15^- isomer, a 32 ns, four-quasiparticle $18^{(+)}$ isomer, and a six-quasiparticle $19^{(-)}$ intrinsic state and its band. Configuration assignments are aided by analysis of the in-band decay properties, which confirm, for example, a predominantly $\nu\pi^3$ configuration for the 15^- isomer. The results are compared with multiquasiparticle calculations. A number of yrast high-K six- and eight-quasiparticle states which could be accessible in future studies are predicted.
[S0556-2813(98)00109-5]

PACS number(s): 21.10.Tg, 23.20.Lv, 27.70.+q, 21.10.Ky

I. INTRODUCTION

The odd-odd nuclide ^{180}Ta has the distinction of being both the least abundant naturally occurring isotope in the solar system, and the only one found as an isomer. The natural form is not the 1^+ ground state which lives for only 8 h, but rather the 75.3 keV 9^- excited state which lives for longer than 1.2×10^{15} yr. Its production in nucleosynthesis has been the subject of conjecture (see, for example, the summary by Schlegel *et al.* [1]).

Early measurements on the ^{180m}Ta (γ,γ') reaction yielded large cross sections leading from the 9^- isomer to the ground state [2–5] implying an intermediate excitation and decay path which would mitigate against its survival in stellar processes. The additional implication that the inelastic excitation through excited intermediate states required K mixing to allow for the change of 8 units in K (the projection of the spin on the nuclear deformation axis) to pass from the isomer to the ground state, is one of the imperatives for studying the spectroscopy of ^{180}Ta, of which little was known until recently. Measurements have now been reported on photonuclear studies [6] and Coulomb excitation [1,7]. While we would not necessarily expect the same states involved in (γ,γ') excitations or Coulomb excitation to be identified in the present measurements, some connecting paths might be accessible. In any case, a comprehensive level scheme is a prerequisite input to theoretical calculations for ^{180}Ta, which will be required to understand the processes involved. A second imperative relates to our systematic experimental and theoretical studies of multiquasiparticle states in a range of tantalum isotopes [8–13]. With $N=107$, ^{180}Ta is at the edge of the $N=108$ subshell, so that the character of the neutron particle and hole orbitals which must be combined to make multiquasiparticle states, will differ from that in the lighter isotopes.

Earlier we reported [13] the identification of a 45 μs 15^- isomer in ^{180}Ta and its decay through members of the 9^- rotational band. The isomer was observed in ^{11}B-induced reactions, primarily aimed at the study of ^{183}Re, but in which α emission leads to tantalum products, particularly ^{180}Ta and ^{181}Ta. The opportunity of studying the spectroscopy of tantalum isotopes so close to stability, at moderate angular momentum, has been pursued using α-γ coincidences to select the weaker channels. Complementary measurements using ^{7}Li-induced reactions to favor the population of low spin states have also been carried out.

II. EXPERIMENTAL TECHNIQUES

Excited states in ^{180}Ta were populated using ^{11}B and ^{7}Li bombardments of 4.6 mg/cm^2 and 2.0 mg/cm^2 metallic targets of ^{176}Yb. As detailed in Ref. [13], some information was obtained on ^{180}Ta from γ-γ-time studies constrained to the time region between beam pulses, giving sensitivity to states populated through long-lived isomers. The present measurements with ^{11}B were designed to select directly the weak $\alpha 3n$ and $\alpha 2n$ exit channels leading to ^{180}Ta and ^{181}Ta, by demanding coincidences with α particles. One set of particle-γ-γ-time measurements was carried out at a beam energy of 55 MeV, with ^{11}B beams from the ANU 14UD accelerator, the energy optimum for $4n$ evaporation. Excitation functions were carried out, in coincidence with α particles, over a range of energies from 45 to 75 MeV to confirm the isotopic assignments. From these, peak energies for channels involving α emission were found to be higher than for channels involving only neutron emission, as expected and as discussed below. A second measurement was therefore carried out at 65 MeV. A third set of measurements was carried out using the (^{7}Li,$3n$) reaction at an energy of 28 MeV, below the nominal Coulomb barrier to populate pref-

erentially low-spin states, as an independent means of assignment.

A. γ-ray array

All γ-ray measurements were carried out with the CAESAR array which contains six Compton-suppressed detectors when the particle-detector ball is included, and an additional two LEPS detectors when it is not (as was the case for the ^{7}Li induced reactions). The Compton-suppressed detectors are arranged in the vertical plane containing the beam axis, with detectors at pairs of angles of approximately $\pm 48°$, $\pm 97°$, and $\pm 145°$. It is of particular importance for the present measurements that both energy and time information is recorded for all γ-ray detectors, allowing the isolation of isomers of a few nanoseconds and longer, and therefore the temporal ordering of parts of the level scheme. It is also of importance that minimal absorbers are used and appropriate care is taken with time restrictions, etc., so that all detectors in the array have useable efficiencies down to 35 keV, extending to about 20 keV for the LEPS detectors.

B. Lifetimes and time correlations

State lifetimes were extracted from a number of sources including particle-γ-time measurements and the various combinations of γ-γ-time data, which allowed isolation of specific levels by gating on transitions directly above and below the states of interest. In the case of relatively low-energy transitions, it was possible in the lower-spin input ^{7}Li-induced reaction to choose between gating using the HpGe detectors or the LEPS detectors, the latter of which have superior timing resolution.

By gating on specific time regions depending on whether transitions are delayed or prompt, it is possible to identify unambiguously transitions feeding and following isomers. In the analyses, a number of different conditions were used to optimize specific isomers. For states with relatively short lifetimes (in the region of 20 ns), significant intensity will remain in the time regions notionally identified as ''prompt.'' More stringent gates could be applied when using the LEPS detectors.

C. Particle-γ coincidences

Charged particles were detected in a compact array of scintillators inserted inside CAESAR. The particle array contains 14 fast/slow plastic combinations for which the phoswich technique is used to separate fast signals in the thin front element (ΔE) from the thicker (slow) rear element (E), allowing particle identification to be performed. The array covers approximately 85% of 4π, and there are three rings of essentially equivalent particle detectors, four ''forward,'' six ''middle,'' and four ''backward,'' subtending angular ranges of approximately 20° to 60°, 60° to 120°, and 120° to 165°. For the present experiments, gold absorber foils of 82 mg/cm^2 were used on the four forward detectors to reduce the flux from scattered beam particles.

Hardware gates were set to select α particles and to discriminate against protons and scattered boron ions. In the later measurements time-filtered ΔE signals [14] were recorded for gating, and in some of these the signals from the three rings of detectors were recorded to allow selection between the angles of α emission. Under these conditions there are limitations because of the limited granularity and coarse angular resolution, and a reduction in efficiency occurs for low-energy α particles because of absorbers on the forward detectors.

D. Reaction mechanisms

The peak energy for production of the nucleus ^{180}Ta in the ^{176}Yb $(^{7}\mathrm{Li},3n)^{180}$Ta reaction is expected to be at about 32 MeV, close to the nominal Coulomb barrier of about 29 MeV and hence a low angular momentum input is expected. In the measurement carried out the energy was reduced even further, to 28 MeV, which resulted in about equal yield of ^{179}Ta $(4n)$ and ^{180}Ta and essentially no yield of ^{181}Ta $(2n)$.

Much higher spin input, and a different population pattern, was achieved by exploiting the so-called ''massive transfer'' or ''incomplete fusion'' reaction [15,16] in which (in simplified terms) the breakup of ^{11}B into ^{7}Li and an α particle is followed by fusion of the ^{7}Li fragment with ^{176}Yb. The mechanism is more complicated than a simple breakup, but the important point is that the angular momentum input can be higher, being somewhere between that corresponding to peripheral capture of ^{11}B, giving $l_{\max}\sim 25\hbar$ at 60 MeV, or of the ^{7}Li fragment, giving $l_{\max}\sim 16\hbar$. The breakup component may have a narrow-l distribution, corresponding to selection of grazing impact parameters.

The optimum ^{11}B beam energy required for such a process can be estimated by allowing for the α-^{7}Li separation energy of 8.7 MeV and by assuming that the kinetic energy is shared between the fragments, so that the optimum energy would be at $\sim 11/7(32+8.7)=63$ MeV, as substantiated by the excitation functions. Similarly, significant production of ^{181}Ta which would not be possible with the $(^{7}\mathrm{Li},2n)$ reaction because it is too far below the Coulomb barrier, does occur with the $(^{11}\mathrm{B},\alpha 2n)$ reaction at 55 MeV.

In the ^{11}B induced reactions, population of the tantalum isotopes can occur either via the evaporation of α particles or by the incomplete fusion processes discussed above. From statistical model calculations the former process is expected to be weak, whereas the latter results in cross sections which are of the order of $\sim 10\%$ of the main xn evaporation channels. The former process also gives isotropic α-particle emission in the center of mass, whereas the incomplete fusion is in general, more forward peaked. In detail, it is likely to be correlated with the projectile grazing angles which can be backwards of 90° at the lowest beam energies, moving forward to about 30° at the highest energies.

Under the conditions of the present experiments with lower efficiency for detection of lower-energy α particles emitted at forward angles, the yields of particular isotopes are also correlated with the angle of emission of the α-particle. This allows a coarse differentiation between reaction channels, the heavier product (fewer neutrons emitted) being associated with more forward α emission, with that pattern moving progressively towards more forward angles as the beam energy is raised, as discussed recently [19].

E. Assignment to ^{180}Ta

Strong transitions in ^{180}Ta were identified initially by their coincidences with tantalum x rays, with due regard for

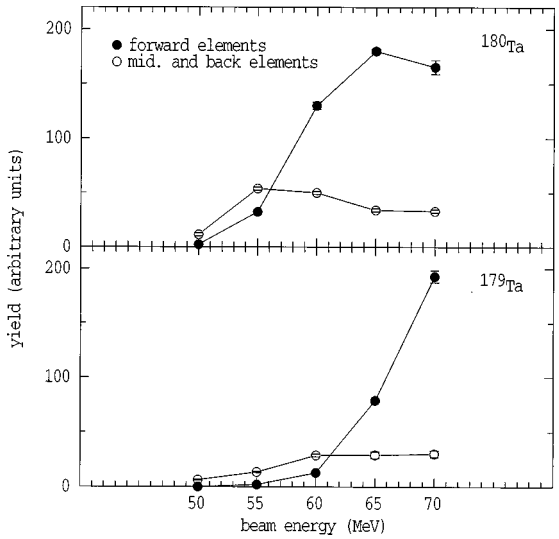

FIG. 1. Yields of transitions representative of ^{180}Ta and ^{179}Ta observed in the ^{11}B-induced reactions separated into coincidences with α particles detected in either the forward elements or the other elements of the particle-detector ball.

the transitions known to be in ^{179}Ta, for which we have established a comprehensive scheme [11], and from the differences in population obtained from the excitation functions and cross bombardments. As well, when separated into coincidences with α particles in the forward detector ring, or the sum of the middle and backward rings, the ^{180}Ta and ^{179}Ta yields have different energy dependences, as shown in Fig. 1. The yield into the middle and backward rings is more constant, and the forward yield for ^{180}Ta increases more rapidly than that for ^{179}Ta, as the beam energy increases. The other tantalum product ^{181}Ta is essentially only observed at the lowest energies, and only in coincidence with α particles in the forward ring.

Once some transitions and states were established, such as the 8^+ state at 176 keV seen in the decay of ^{180}Hf [18], but for which we have measured a lifetime of 101 ns, early delayed coincidences could be used to identify unambiguously all transitions feeding it. In this context, the long lifetime of the 15^- isomer precludes easy identification of transitions feeding it, but they were placed with reliability on the basis of the excitation functions carried out in the ^{11}B induced reactions, in coincidence with α particles.

III. LEVEL SCHEME AND RESULTS

The level scheme deduced from the present work is given in three parts, in Figs. 2, 3, and 4. The transitions and their properties are listed in Table I, with indicative intensities only since they are drawn from a number of measurements with differing populations. In-band γ-ray branching ratios are listed in Tables II and III, and the lifetimes measured in the present work, with corresponding transition strengths are given in Table IV.

In constructing the schemes, the information assumed from previous work is the existence of the 75.3 keV 9^-

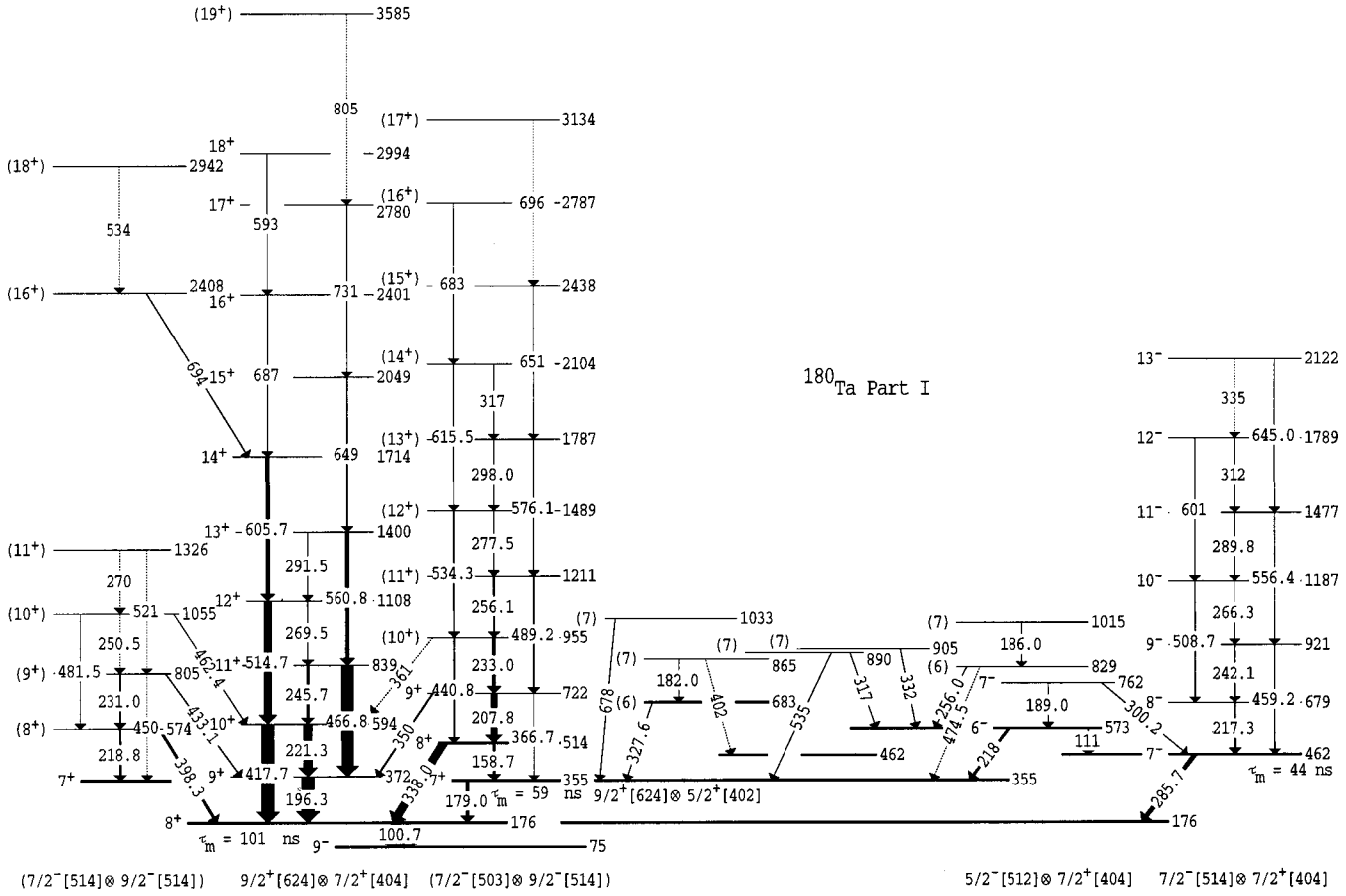

FIG. 2. Part I of the ^{180}Ta level scheme; transitions feeding to the 9^- state through the 8^+ isomer.

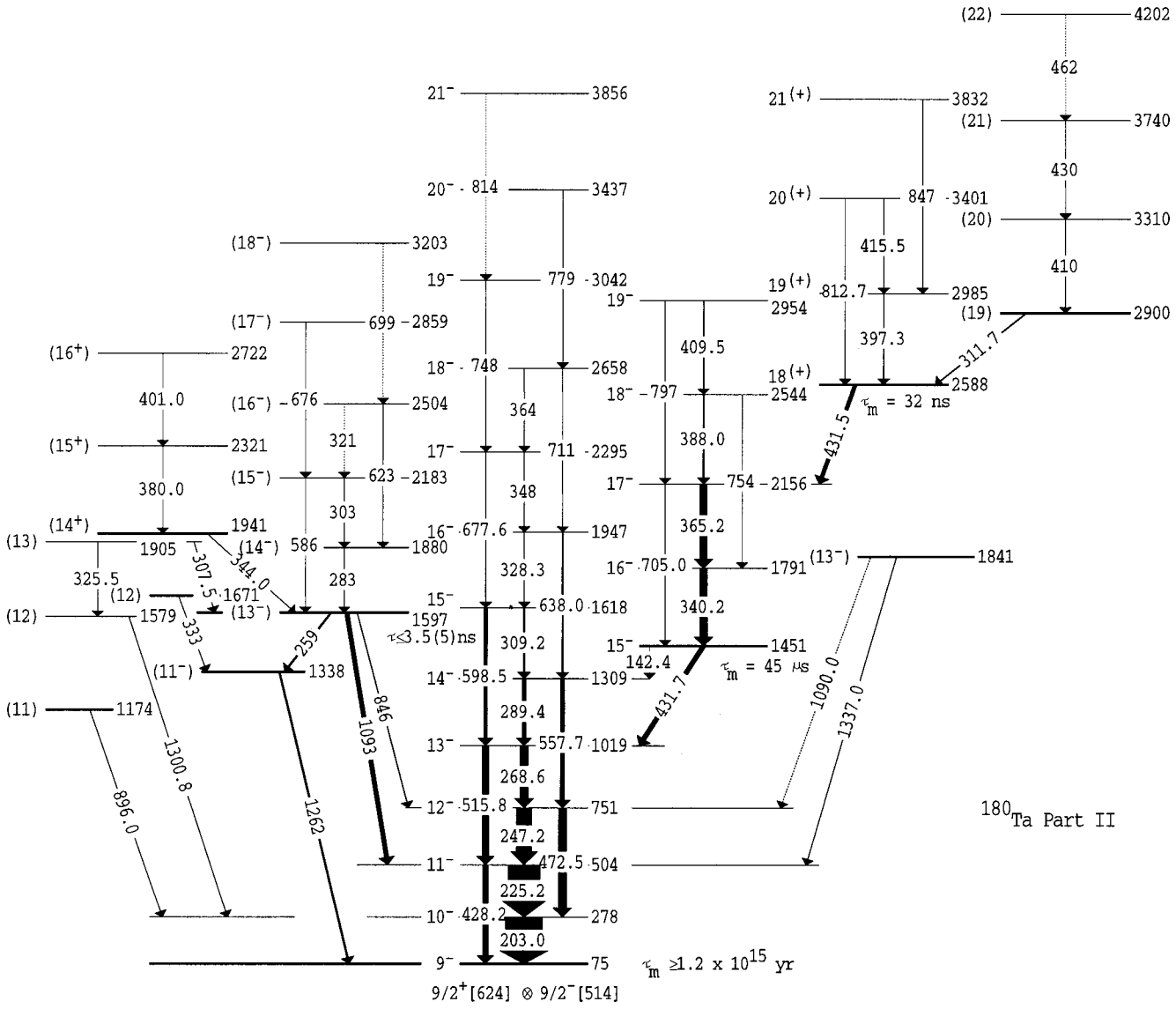

FIG. 3. Part II of the ^{180}Ta level scheme; transitions feeding the 9^- and 15^- isomers.

isomer and a 1^+ ground state. The energy of the 9^- isomer given in the most recent compilation [17], has not been measured directly but is deduced from mass differences with a quoted error of 1.3 keV. A 100.7 keV transition known from the ^{180}Hf β decay [18] was placed as feeding the 9^- isomer, from an 8^+ state at 176 keV. The $E1$ character of the same transition observed in the present in-beam study is established by the total conversion coefficient deduced from intensity balances. Most other prior information available was from particle-transfer reactions, as summarized in the recent compilation [17] with consequent lower precision in energy and tentative spin assignments. As will be discussed below, most of the intrinsic states identified here, and some of the rotational band members, have counterparts in states assigned previously. However the high level density means that some of the peaks observed in the particle-transfer reactions are multiple.

Spin assignments have been made considering the decays and interconnections, the anisotropies obtained for some transitions in both the ^{7}Li induced reaction and in coincidence with α particles in the ^{11}B-induced reaction, and the total conversion coefficients, obtained mainly from intensity balances.

A. States feeding through the 8^+ isomer at 176 keV

A time spectrum gated on transitions feeding this isomer and stopping on the 100.7 keV transition is shown in Fig. 5(a), with a fit from which the lifetime was extracted. An example of a spectrum showing the transitions which precede the 100.7 keV transition in time is given in Fig. 6(a), in this case from the ^{11}B induced measurement at 55 MeV. The spectrum of transitions delayed with respect to those which feed the 8^+ isomer is not shown but it confirms that the decay proceeds by a single transition. The γ rays in Fig. 6(a) are from the rotational band based on the isomer and from a number of other states, some without apparent band structures, others from well defined states and bands as shown in the partial scheme in Fig. 2.

The time correlated gate on the 286 transition, which feeds the 176 keV isomer [Fig. 6(b)], selects transitions preceding this γ ray. The 286 keV transition itself depopulates a

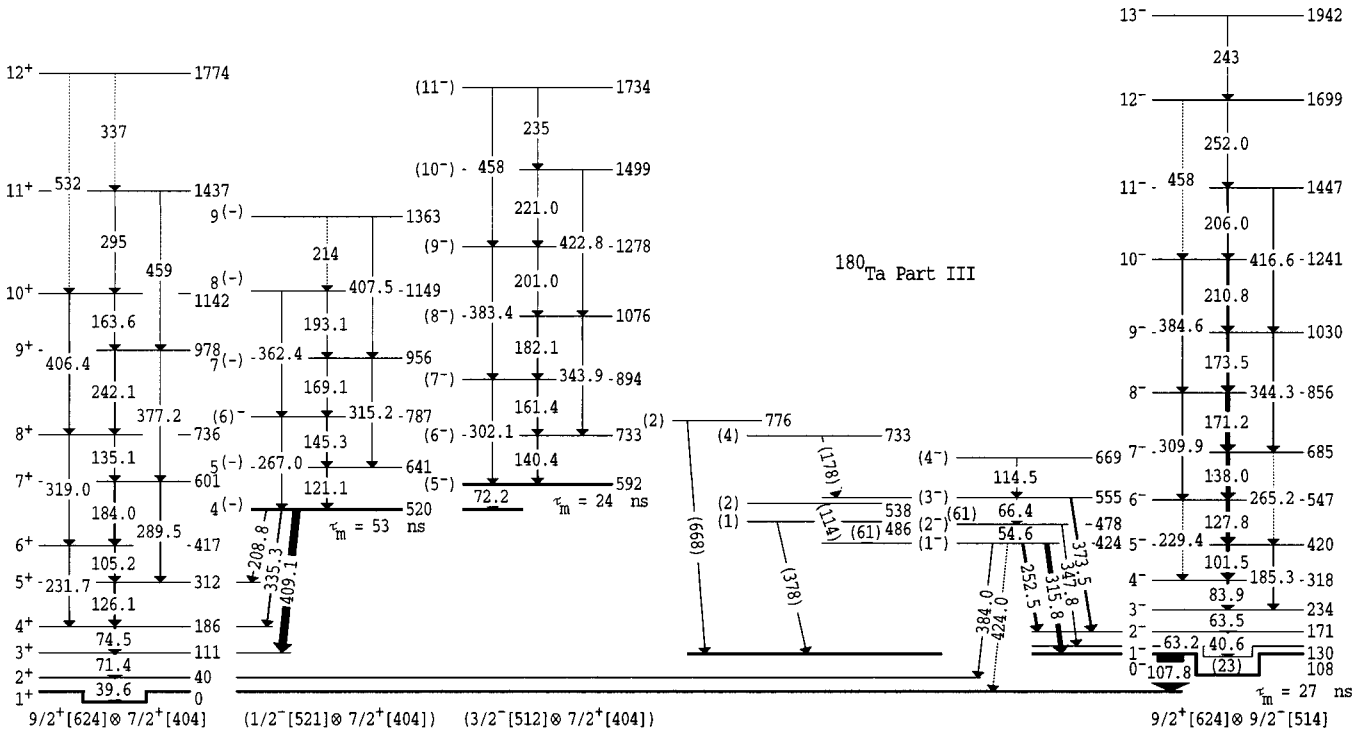

FIG. 4. Part III of the ^{180}Ta level scheme; transitions associated with the 1^+ ground state and bands which feed it.

44 ns isomer as determined from the time spectrum in Fig. 5(b). The main transitions in Fig. 6(b) are the members of the band based on the 462 keV intrinsic state as well as the 111 keV transition which feeds from a 573 keV state. The 111 keV transition must be $M1$ from its total conversion coefficient. The 286 keV transition which depopulates the 462 keV isomer has a negative A_2 coefficient suggesting a stretched dipole character, which, together with the low population of the state and its band, suggests spin 7. The delayed intensity balance favors $E1$ character, although at 286 keV the total conversion coefficients are small, being 0.02 for $E1$ and 0.23 for $M1$. Negative parity has been assumed which also leads to negative parity for the 573 keV state. That state is unlikely to be 7^- or 8^- given its weak population. The intensity in the band based on this state drops rapidly, even in the ^{7}Li-induced reaction, making it difficult to assign higher states and thus characterize the band, favoring the low spin (6^-) suggested.

The prompt gate on the 338 keV transition which connects the 514 keV state to the 176 keV isomer exhibits a single rotational band, as shown in Fig. 6(c). Higher members of the same band also have connecting transitions to the 8^+ band. The 338 keV transition has a positive A_2 coefficient consistent with a $J\rightarrow J$ or mixed $\Delta J=1$ $(E2/M1)$ transition. (Note that the value obtained is from the ^{7}Li reaction where the close-lying 340 keV transition from the 15^- band is not populated because of the low spin input.) The 514 keV state is suggested to be 8^+ although 7^+ remains a less-likely possibility. The relatively strong population favors the higher spin which would make the states of the band relatively more yrast than those of the 7^- band. Although it is not shown on the level scheme, there is some evidence for a 439 keV transition connecting the 514 keV state and the 9^- 75 keV isomer, which if confirmed, would eliminate the 7^+ possibility.

The lifetime of the 514 keV state must be short, as can be seen, for example, from the intermediate time spectrum shown in Fig. 5(c). The spectrum was obtained by gating on higher transitions and the other main decay branch at 159 keV which connects it to a state at 355 keV. That state decays via a 179 keV transition and has a 59 ns lifetime, as can be seen from Fig. 5(d) which shows the time spectrum analogous to that in Fig. 5(c), but with the 159 keV transition replacing the 179 keV transition as ''stop.''

Assignment of the 355 keV level as a spin 7 intrinsic state is consistent with dipole character for the 179 keV transition to the 8^+ 176 keV state. Conversion coefficient limits from intensity balances suggest $M1$ for both the 159 and 179 keV transitions giving spin and parity of 7^+ for the 355 keV state and consistent with 8^+ (or 7^+) for the 514 keV state.

As can be seen from Fig. 6(d) the 355 keV isomeric state is fed by a number of transitions but these do not form a clear rotational band. In attempting to establish such a band, a number of possibilities have been considered: (a) that the states on the extreme left of Fig. 2 beginning with the 574 keV state could be the higher members, (b) that the 514 keV state and the states above it form the band, (c) that some of the other transitions from a number of states (those in the middle part of Fig. 2) are from band members.

Considering possibility (a), except for the 574 keV state which decays by the 218.8 keV transition to the 355 keV state and also by the 398.3 keV transition to the 176 keV state, the band is weakly populated and hence not well defined. In favor of the proposition is the fact that the state energies correspond to a regular sequence, and the fact that the 574 keV state does not exhibit a significant lifetime, so that it might not be an intrinsic state. On the other hand, its apparently fast decay via a 398 keV transition to the 8^+ intrinsic state at 176 keV is unexpected if it were a member of the 355 keV band, given the retarded nature of the 179

TABLE I. Transitions assigned to ^{180}Ta.

E_γ	I_γ	A_2/A_0 [a]	E_i	E_f	J_i^π,K_i	J_f^π,K_f
(23)			130.4	107.8	(1^-),0	0^-,0
39.6	95(22)		39.6	0.0	2^+,1	1^+,1
40.6	110(20)		171.0	100.4	2^-,0	1^-,0
54.6	140(30)		478.2	423.6	(2^-),1	(1^-),1
(61)			486.0	423.6	(1)	1^-,1
(61)			538.1	478.2	(2)	(2^-),1
63.2	~15		171.0	107.8	2^-,0	0^-,0
63.5	367(30)		234.1	171.0	3^-,0	2^-,0
66.4	~70		554.6	478.2	3^-,1	(2^-),1
71.4	220(40)		111.0	39.6	3^+,1	2^+,1
72.2	~15		592.4	520.2	(5^-),5	$4^{(-)}$,4
74.5	~140		185.5	111.0	4^+,1	3^+,1
83.9	120(15)		318.1	234.1	4^-,0	3^-,0
100.7	1300(120)	−0.06(5)	176.0	75.3	8^+,8	9^-
101.5	205(15)		419.6	318.1	5^-,0	4^-,0
105.2	67(11)		416.8	312.0	6^+,1	5^+,1
107.8	1600(120)	−0.01(3)	107.5	0.0	0^-,0	1^+,1
111.0	~60		572.9	461.7	6^-	7^-,7
(114)			538.1	423.6	(2)	1^-,1
114.5	78(21)		669.1	554.6	(4^-)	(3^-)
121.1	70(12)		641.3	520.2	$5^{(-)}$,4	$4^{(-)}$,4
126.1	99(15)		312.0	185.5	5^+,1	4^+,1
127.8	240(22)	−0.31(13)	547.4	419.6	6^-,0	5^-,0
135.1	29(8)		736.0	600.8	8^+,1	7^+,1
138.0	231(30)	−0.19(9)	685.4	547.4	7^-,0	6^-,0
140.4	95(10)	+0.29(15)	732.8	592.4	(6^-),5	(5^-),5
142.4	30(7)		1451.0	1308.7	15^-,15	14^-,9
145.3	58(8)		786.6	641.3	$6^{(-)}$,4	$5^{(-)}$,4
158.7	64(9)		513.7	355.0	(8^+),7	7^+,7
161.4	73(7)		894.2	732.8	(7^-),5	(6^-),5
163.6	21(4)		1141.6	978.0	10^+,1	9^+,1
169.1	26(5)		955.7	786.6	$7^{(-)}$,4	$6^{(-)}$,4
171.2	250(23)	−0.20(9)	856.4	685.4	8^-,0	7^-,0
173.5	188(19)	−0.10(23)	1029.9	856.4	9^-,0	8^-,0
(178)			732.6	554.6	(4)	(3^-)
179.0	164(12)	−0.14(3)	355.0	176.0	7^+,7	8^+
182.0	7(2)		865.0	682.6	(7)	(6)
182.1	34(9)		1076.3	894.2	(8^-),5	(7^-),5
184.0	101(16)	[+0.21(12)]	600.8	416.8	7^+,1	6^+,1
185.3	32(5)		419.6	234.1	5^-,0	3^-,0
186.0	5(2)		1015.0	829.0	(7)	(6)
189.0	5(2)		761.9	572.9	7^-	6^-
193.1	13(3)		1149.0	955.7	$8^{(-)}$,4	$7^{(-)}$,4
196.3	262(18)	+0.02(7)	372.3	176.0	9^+,8	8^+,8
201.0	15(3)		1277.6	1076.3	(9^-),5	(8^-),5
203.0	2158(80)	+0.20(7)	278.3	75.3	10^-,9	9^-,9
206.0	85(14)		1447.0	1240.7	11^-,0	10^-,0
207.8	62(13)		721.5	513.7	(9^+),7	(8^+),7
208.8	55(6)		520.2	311.6	$4^{(-)}$,4	5^+,1
210.8	160(15)	−0.45(24)	1240.7	1029.9	10^-,0	9^-,0
214	~6		1363.2	1149.0	$9^{(-)}$,4	$8^{(-)}$,4
217.3	44(6)		679.0	461.7	8^-,7	7^-,7
218.0	51(6)		572.9	355.0	(6^-)	7^+
218.8	24(3)		573.8	355.0	(8^+),8	7^+,7
221.0	8(2)		1499.1	1277.6	(10^-),5	(9^-),5

TABLE I. (*Continued*).

E_γ	I_γ	A_2/A_0 [a]	E_i	E_f	J_i^π,K_i	J_f^π,K_f
221.3	90(16)		593.6	372.3	10^+,8	9^+,8
225.2	1418(90)	+0.17(9)	503.5	278.3	11^-,9	10^-,9
229.4	32(4)		547.4	318.1	6^-,0	4^-,0
231.0	9(2)		804.8	573.8	(9^+),8	(8^+),8
231.7	34(4)		416.8	185.5	6^+,1	4^+,1
233.0	33(5)		954.5	721.5	(10^+),7	(9^+),7
235	~4		1734.2	1499.1	(11^-),5	(10^-),5
242.1	20(4)		921.1	679.0	9^-,7	8^-,7
242.1	48(6)		978.0	736.0	9^+,1	8^+,1
243.0	~30		1942.0	1699.0	13^-,0	12^-,0
245.7	24(3)		839.1	593.6	11^+,8	10^+,8
247.2	670(40)	+0.20(9)	750.7	503.5	12^-,9	11^-,9
250.5	~8		1055.3	804.8	(10^+),8	(9^+),8
252.0	40(6)		1699.0	1447.0	12^-,0	11^-,0
252.5	136(17)	[−0.18(4)]	423.6	171.0	(1^-),1	2^-,0
256.0	12(4)		829.0	573.0	(6)	6^-
256.1	15(3)		1210.7	954.5	(11^+),7	(10^+),7
258.5	120(30)	[−0.18(15)]	1596.5	1337.8	(13^-),13	(11^-)
265.2	34(8)		685.4	419.6	7^-,0	5^-,0
266.3	10(2)		1187.3	921.1	10^-,7	9^-,7
267.0	18(3)		786.6	520.2	$6^{(-)}$,4	$4^{(-)}$,4
268.6	480(25)	+0.10(5)	1019.3	750.7	13^-,9	12^-,9
269.5	20(3)		1108.4	839.1	12^+,8	11^+,8
270.0	~5		1326.0	1055.3	(11^+),8	(10^+),8
277.5	10(3)		1488.8	1210.7	(12^+),7	(11^+),7
283.1	60(10)		1879.5	1596.5	(14^-),13	(13^-),13
285.7	163(22)	−0.13(4)	461.7	176.0	7^-,7	8^+,8
289.4	204(25)		1308.7	1019.3	14^-,9	13^-,9
289.5	57(9)		600.8	312.0	7^+,1	5^+,1
289.8	4(2)		1477.1	1187.3	11^-,7	10^-,7
291.5	6(2)		1400.0	1108.4	13^+,8	12^+,8
295	25(6)		1437.0	1141.6	11^+,1	10^+,1
298.0	5(1)		1786.8	1488.8	(13^+),7	(12^+),7
300.2	17(3)		761.9	461.7	7^-	7^-,7
302.1	20(4)		894.2	592.4	(7^-),5	(5^-),5
303	~15		2182.5	1879.5	(15^-),13	(14^-),13
307.5	~30		1904.6	1596.5	(13)	(13^-),13
309.2	109(15)		1617.8	1308.7	15^-,9	14^-,9
309.9	63(11)		856.4	547.4	8^-,0	6^-,0
311.7	110(15)	[−0.40(17)]	2899.6	2587.9	19^+,19	$18^{(+)}$,18
312	~4		1789.0	1477.1	12^-,7	11^-,7
315.2	20(6)		955.7	641.3	$7^{(-)}$,4	$5^{(-)}$,4
315.8	263(20)	−0.11(3)	423.6	107.8	1^-,1	0^-,0
317	~2		2104.3	1786.8	(14^+),7	(13^+),7
317	5(2)		890.0	572.9	(7)	(6^-)
319.0	39(7)		736.0	416.8	8^+,1	6^+,1
321	~10		2503.5	2182.5	(16^-),13	(15^-),13
325.5	~35		1904.6	1579.1	(13)	(12)
327.6	25(3)		682.6	355.0	(6)	(7^+)
328.3	62(10)		1946.7	1617.8	16^-,9	15^-,9
332	6(2)		905.0	572.9	(7)	(6^-)
333	22(6)		1671.0	1338.0	(12)	(11^-)
335	~2		2122.0	1789.0	13^-,7	12^-,7
335.3	68(8)		520.2	185.5	$4^{(-)}$,4	4^+,1
337	~5		1774.0	1437.0	12^+,1	11^+,1

TABLE I. (*Continued*).

E_γ	I_γ	A_2/A_0 [a]	E_i	E_f	J_i^π, K_i	J_f^π, K_f
338.0	192(15)	+0.35(5)	513.7	176.0	(8^+),7	8^+,8
340.2	221(18)	+0.28(12)	1791.2	1451.0	16^-,15	15^-,15
343.9	52(8)		1076.3	732.8	(8^-),5	(6^-),5
344.0	80(15)		1940.5	1596.5	(14^+)	(13^-),13
344.3	~54(10)		1029.9	685.4	9^-,0	7^-,0
347.8	38(8)		478.2	130.4	(2^-),1	1^-,0
348	24(7)		2295.4	1946.7	17^-,9	16^-,9
350.0	28(7)		721.5	372.3	(9^+),7	9^+,8
(361)			954.5	593.6	(10^+),7	10^+,8
362.4	17(3)		1149.0	786.6	$8^{(-)}$,4	$6^{(-)}$,4
364	~10		2658.0	2295.4	18^-,9	17^-,9
365.2	116(16)	−0.06(4)	2156.4	1791.2	17^-,15	16^-,15
366.7	8(2)		721.5	355.0	(9^+),7	7^+,7
373.5	36(5)		554.6	171.0	(3^-),1	2^-,0
377.2	24(5)		978.0	600.8	9^+,1	7^+,1
(378)			486.0	107.8	(1)	0^-,0
380.0	40(9)		2320.5	1940.5	(15^+),14	(14^+),14
383.4	25(3)		1277.6	894.2	(9^-),5	(7^-),5
384.0	~10		423.6	39.6	(1^-),1	2^+,1
384.6	38(8)		1240.7	856.4	10^-,0	8^-,0
388.0	22(3)		2544.4	2156.4	18^-,15	17^-,15
397.3	88(7)		2985.2	2587.9	(19^+),18	(18^+),18
398.3	56(7)		573.8	176.0	(8^+),8	8^+,8
401.0	~30		2721.5	2320.5	(16^+),14	(15^+),14
(402)			865.0	461.7	(7)	7^-
406.4	30(6)		1141.6	736.0	10^+,1	8^+,1
407.5	~8		1363.2	955.7	$9^{(-)}$,4	$7^{(-)}$,4
409.1	448(120)	−0.16(5)	520.2	111.0	(4^-),4	3^+,1
409.5	~15		2953.9	2544.4	19^-,15	18^-,15
410	~22		3309.6	2899.6	(20^-),19	$19^{(-)}$,19
415.5	5(1)		3400.7	2985.2	(20^+),18	(19^+),18
416.6	32(7)		1447.0	1029.9	11^-,0	9^-,0
417.7	150(13)	+0.24(7)	593.6	176.0	10^+,8	8^+,8
422.8	14(4)		1499.1	1076.3	(10^-),5	(8^-),5
(424.0)			423.6	0.0	(1^-),1	1^+,1
428.2	365(30)	+0.33(10)	503.5	75.3	11^-,9	9^-,9
430	~30		3739.6	3309.6	(21^+),19	(20^+),19
431.5	229(15)	−0.20(6)	2587.9	2156.4	$18^{(+)}$,18	17^-,15
431.7	400		1451.0	1019.3	15^-,15	13^-,9
(433.1)	~10		804.8	372.3	(9^+),8	9^+,8
440.8	18(3)		954.5	513.7	(10^+),7	(8^+),7
450	~4		804.8	355.0	(9^+)	7^+
458	~10		1734.2	1277.6	(11^-),5	(9^-),5
(458.0)			1699.0	1240.7	12^-,0	10^-,0
459	~15		1437.0	978.0	11^+,1	9^+,1
459.2	13(3)		921.1	461.7	9^-,7	7^-,7
(462)			4201.6	3739.6	(22^-),19	(21^-),19
(462.4)			1055.3	593.6	(10^+),8	10^+,8
466.8	130(18)		839.1	372.3	11^+,8	9^+,8
472.5	412(20)	+0.17(7)	750.7	278.3	12^-,9	10^-,9
474.5	15(3)		829.0	355.0	(6)	7^+
481.5	16(3)		1055.3	573.8	(10^+),8	(8^+),8
489.2	18(3)		1210.7	721.5	(11^+),7	(9^+),7
508.7	10(3)		1187.3	679.0	10^-,7	8^-,7
514.7	110(15)		1108.4	593.6	12^+,8	10^+,8

TABLE I. (*Continued*).

E_γ	I_γ	A_2/A_0 [a]	E_i	E_f	J_i^π, K_i	J_f^π, K_f
515.8	500(35)	+0.19(14)	1019.3	503.5	13^-,9	11^-,9
(521)			1326.0	804.8	(11^+)	(9^+)
(532)			1774.0	1141.6	12^+,1	10^+,1
(534)			2942.0	2408.0	(18^+)	(16^+)
534.3	14(3)		1488.8	954.5	(12^+),7	(10^+),7
535	12(3)		890.0	355.0	(7)	7^+
556.4	11(2)		1477.1	921.1	11^-,7	9^-,7
557.7	337(22)	+0.37(13)	1308.7	750.7	14^-,9	12^-,9
560.8	61(9)		1400.0	839.1	13^+,8	11^+,8
576.1	9(3)		1786.8	1210.7	(13^+),7	(11^+),7
586	~40		2182.5	1596.5	(15^-),13	(13^-),13
593	10(3)		2994.0	2401.0	18^+,8	16^+,8
598.5	220(20)		1617.8	1019.3	15^-,9	13^-,9
601	~7		1789.0	1187.3	12^-,7	10^-,7
605.7	56(9)		1714.0	1108.4	14^+,8	12^+,8
615.5	9(2)		2104.3	1488.8	(14^+),7	(12^+),7
623	26(3)		2503.5	1879.5	(16^-),13	(14^-),13
638.0	120(15)		1946.7	1308.7	16^-,9	14^-,9
645.0	~4		2122.0	1477.1	13^-,7	11^-,7
649	20(4)		2049.0	1400.0	15^+,8	13^+,8
651	6(2)		2437.8	1786.8	(15^+),7	(13^+),7
668	~10		775.8	107.8	(2)	0^-,0
676	~20		2859.0	2182.5	(17^-),13	(15^-),13
677.6	110(18)		2295.4	1617.8	17^-,9	15^-,9
678	14(2)		1033.0	355.0	(7)	7^+
683	5(1)		2787.0	2104.3	(16^+),7	(14^+),7
687	15(3)		2401.0	1714.0	16^+,8	14^+,8
694	23(4)		2408.0	1714.0	(16^+)	14^+,8
696.0	3(1)		3134.0	2437.8	(17^+),7	(15^+),7
(699)			3203.0	2503.5	(18^-),13	(16^-),13
705.0	14(2)		2156.4	1451.0	17^-,15	15^-,15
711	~60		2658.0	1946.7	18^-,9	16^-,9
731	10(2)		2780.0	2049.0	17^+,8	15^+,8
748	45(10)		3042.0	2295.4	19^-,9	17^-,9
754	6(2)		2544.4	1791.2	18^-,15	16^-,15
779	~25		3437.0	2658.0	20^-,9	18^-,9
797	5(1)		2953.9	2156.4	19^-,15	17^-,15
805	~5		3585.0	2780.0	(19^+),8	17^+,8
812.7	6(1)		3400.7	2587.9	(20^+),18	(18^+),18
814	~20		3856.0	3042.0	21^-,9	19^-,9
846	74(18)		1596.5	750.7	(13^-),13	12^-,9
847	~7		3832.0	2985.2	(21^+),18	(19^+),18
896	~80		1174.0	278.3	(11)	10^-,9
1090	~60		1841.0	750.7	(13^-)	12^-,9
1093	260(25)	+0.23(9)	1596.5	503.5	(13^-),13	12^-,9
1262	220(30)		1337.8	75.3	(11^-)	9^-,9
1300.8	~100		1579.1	278.3	(12)	10^-,9
1337	~60		1841.0	503.5	(13^-)	11^-,9

[a]Parentheses indicate possible residual contaminant.

keV transition to the 176 keV state.

Possibility (b) was also considered since the 514 keV state is not isomeric hence it also might not be an intrinsic state. Again this possibility has the problem of a (relatively) fast branch via the 338 keV transition to the 8^+ bandhead, in contrast to the retarded nature of the 179 keV transition to the same state. Also, if this were the correct assignment the $8^+ \rightarrow 7^+$ transition energy of 159 keV is low, implying dis-

TABLE II. Branching ratios and $(g_K - g_R)/Q_0$ values for bands in ^{180}Ta.

J^π	$E_\gamma(\Delta I=1)$ (keV)	$E_\gamma(\Delta I=2)$ (keV)	λ [a]	$\lvert g_K - g_R \rvert$ [b] exp.	theory
$K^\pi = 9^-$	75 keV				+ 0.27
15^-	309.2	598.5	2.0(3)	0.270(23)	
14^-	289.4	557.7	1.25(12)	0.305(16)	
13^-	268.6	515.8	0.94(10)	0.294(18)	
12^-	247.2	472.5	0.44(3)	0.345(12)	
11^-	225.2	428.2	0.29(2)	0.281(12)	
$K^\pi = 8^+$	176 keV				− 0.08
13^+	291.5	560.8	5.2(18)	0.125(60)	
12^+	269.5	514.7	5.0(9)	0.075(36)	
11^+	245.7	466.8	7.4(18)	0.098^{+10}_{-20}	
10^+	221.3	417.7	2.3(4)	0.063^{+14}_{-26}	
$K^\pi = 7^+$	514 keV as 8^+				+ 0.20
13^+	298.0	576.1	1.74(38)	0.397^{+59}_{-43}	
12^+	277.5	534.3	1.40(19)	0.383^{+35}_{-28}	
11^+	256.1	489.2	1.20(14)	0.340^{+26}_{-22}	
10^+	233.0	440.8	0.58(5)	0.393^{+21}_{-19}	
9^+	208.0	(366.7) [c]	0.59(8)	[0.186(23)] [c]	
$K^\pi = 8^+$	514 keV as 8^+				+0.58 or +0.30
13^+	298.0	576.1	1.74(38)	0.306^{+50}_{-36}	
12^+	277.5	534.3	1.40(19)	0.283^{+28}_{-23}	
11^+	256.1	489.2	1.20(14)	0.229^{+21}_{-18}	
10^+	233.0	440.8	0.58(5)	0.222(14)	
$K^\pi = 7^-$	462 keV				+0.19
11^-	289.8	556.4	2.7(9)	0.227^{+73}_{-48}	
10^-	266.3	508.7	1.66(4)	0.231(45)	
9^-	242.0	459.2	1.15(2)	0.165(26)	
$K^\pi = (5^-)$	592 keV				+0.34
10^-	221.0	422.8	1.9(7)	0.397^{+113}_{-65}	
9^-	201.0	383.4	1.6(4)	0.358^{+56}_{-40}	
8^-	182.1	343.9	1.5(2)	0.274^{+27}_{-22}	
7^-	161.4	302.1	0.28(6)	0.165^{+63}_{-47}	
$K^\pi = 4^{(-)}$	520 keV				+0.44
8^-	193.1	362.4	1.3(4)	0.487^{+92}_{-61}	
7^-	169.1	315.2	0.78(16)	0.490^{+63}_{-47}	
6^-	145.3	267.0	0.31(6)	0.519^{+68}_{-50}	
$K^\pi = 1^+$	g.s.				− 3.3
10^+	163.6	406.4	1.4(7)	4.1^{+15}_{-7}	
9^+	242.1	377.2	0.50(2)	3.2^{+10}_{-52}	
8^+	135.1	319.0	1.37(55)	3.0^{+9}_{-5}	
7^+	184.0	289.5	0.56(11)	2.3^{+3}_{-2}	
6^+	105.2	231.7	0.50(13)	3.2^{+5}_{-4}	
$K^\pi = 15^-$	1451 keV				+0.46
20^-	409.5	797	0.25(8)	0.54^{+12}_{-8}	
19^-	388.0	754	0.29(11)	0.42^{+13}_{-7}	
18^-	365.2	705	0.13(4)	0.51^{+10}_{-7}	
$K^\pi = 18^{(+)}$	2588 keV				+0.03
20^+	415.5	812.7	1.0(3)	0.046^{+24}_{-30}	

[a] Branching ratios $\lambda = I_\gamma(I \to I-2)/I_\gamma(I \to I-1)$.
[b] Taking $Q_0 = 6.79(3)$ and $g_R = 0.26$.
[c] If the 355 keV state were the bandhead.

tortion of the level spacing. The large number of transitions connecting the bands in this region could indicate mixing and therefore perturbations are possible but the conceivable scenarios with the present ordering of spins would usually lead to a higher, rather than a lower, transition energy.

The balance of the arguments therefore favors possibility (c). That is, that some of the other transitions which feed the 355 keV state are in fact part of its band, such as those from

TABLE III. Experimental and calculated branching ratios for the 0^- band in ^{180}Ta.

J^π	$E_\gamma(\Delta I=1)$ (keV)	$E_\gamma(\Delta I=2)$ (keV)	λ[a] exp.	λ [b] theory
$K^\pi=0^-$	108 keV			
11^-	206.0	416.6	0.6(2)	0.324
10^-	210.8	384.6	0.30(7)	0.201
9^-	173.5	344.3	0.19(6)	0.203
8^-	171.2	309.9	0.17(6)	0.124
7^-	138.0	265.2	$\leqslant$0.12(4)	0.110
6^-	127.8	229.4	$\leqslant$0.14(5)	0.064
5^-	101.5	185.3	$\leqslant$0.16(3)	0.043
4^-	83.9	(147.4)		0.023
3^-	63.5	(104.2)		0.009

[a]Branching ratios $\lambda = I_\gamma(I\rightarrow I-2)/I_\gamma(I\rightarrow I-1)$.
[b]Taking $Q_0=6.79(3)$.

the states at 573 and 829 keV. Their spins and parities are mostly tentative since only fragmentary band structure is observed, presumably because of their nonyrast nature. That leaves both the 574 and 514 keV states as other bandheads.

B. States feeding through the 9^- and 15^- isomers

Observation of the 15^- 45 μs isomer at 1451 keV and its corresponding decay to the 9^- band was covered in a previous publication [13], from the results of a ^{11}B bombardment but without particle gating. γ-γ coincidence spectra restricted to transitions occurring between beam pulses from that measurement are shown in Fig. 7. The present measurements confirm those results and, as shown in part II of the level scheme (Fig. 3), also allow the identification of states feeding into the lower members of the 9^- band, which is identified to about spin 21. We have placed a collection of states above the 45 μs isomer; the α-gated excitation functions for the associated 340 and 365 keV transitions, are shown in Fig. 8. These confirm assignment of those transitions to ^{180}Ta, and suggest also that they arise from states of relatively high spin, a deduction supported by their absence in the ^{7}Li-induced reaction. α-γ-γ coincidence gates associated with that isolated group of levels are shown in Fig. 9. The states include a 32 ns isomer, decaying via a 431.5 keV transition, as shown in Fig. 3, coincidentally nearly the same energy as the 431.7 keV transition which depopulates the 15^- isomer itself, hence the presence of the 340 and 365 keV transitions in the delayed spectrum of Fig. 7(c), which was

TABLE IV. Measured lifetimes and transition rates in ^{180}Ta.

E_γ (keV)	Mult.	I_γ (rel.)	α_T	$T_m^{\rm exp}$ [a] (ns)	Strength (W.u.)
0^-, 107.8 keV					
107.8	$E1$	100	0.304	27(1)	$6.9(3)\times10^{-6}$
$4^{(-)}$, 520.2 keV					
409.1	$E1$	79(2)	0.0107	53(3)	$6.6(4)\times10^{-8}$
335.3	$E1$	12(2)	0.017		$1.8(4)\times10^{-8}$
208.8	$E1$	9(2)	0.055		$5.6(12)\times10^{-8}$
(5^-), 592 keV					
72.2	$M1$	100	3.2	24(3)	$8(1)\times10^{-4}$
8^+, 176.0 keV					
100.7	$E1$	100	0.362	101(2)	$2.18(4)\times10^{-6}$
7^+, 355.0 keV					
179.0	$M1$	100	0.869	59(4)	$5.0(4)\times10^{-5}$
7^-, 461.7 keV					
285.7	$E1$	100	0.025	44(3)	$2.9(2)\times10^{-7}$
(13^-), 1597 keV					
1093	$E2$	77(5)	0.0036	$\leqslant$3.5(5) ns	$\geqslant1.9(3)\times10^{-3}$
846	$M1$	23(5)	0.014		$\geqslant3.2(9)\times10^{-6}$
$18^{(+)}$, 2588 keV					
431.5	$E1$	100	0.010	32(3)	$1.2(1)\times10^{-7}$

[a]Experimental meanlife: $T_m^\gamma = T_m^{\rm exp}(\Sigma_i I_{\gamma i}(1+\alpha_{ti}))/I_\gamma$.

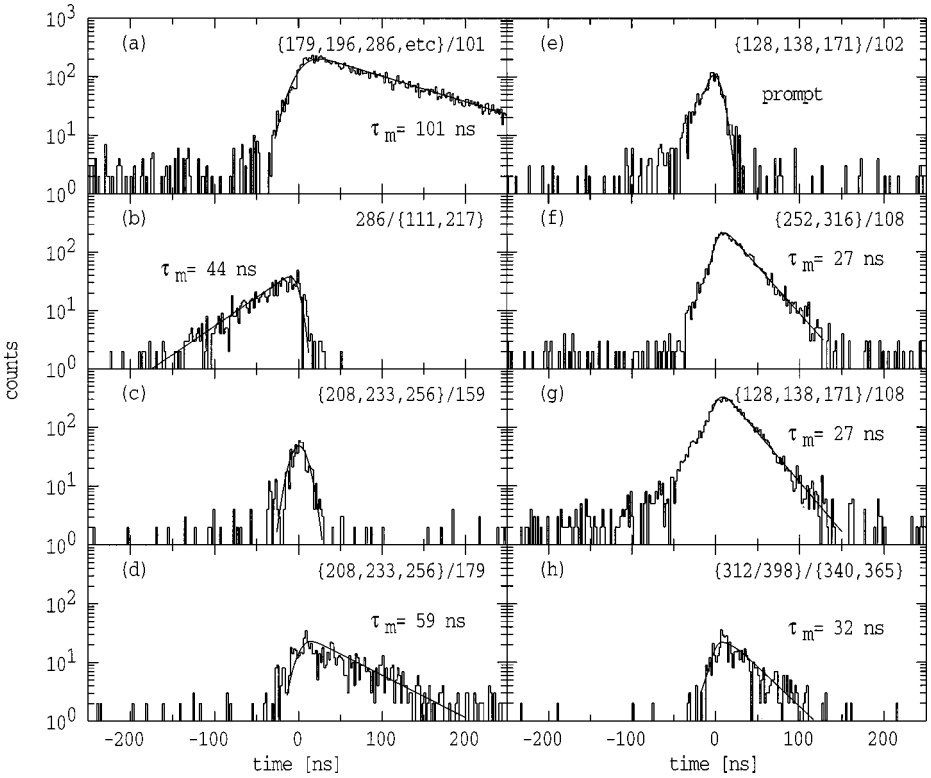

FIG. 5. Time spectra with gates on individual transitions as shown obtained in both the ^{7}Li-induced reaction except for (h) which is from the ^{11}B-induced reaction. The code in each panel indicates the *start/stop* transitions with the ''stop'' detector in the ^{7}Li induced reaction being the LEPS detector which has a better timing response.

obtained with a gate on 432 keV γ rays. The lifetime of 32 ns for the 2588 keV state is evident in the time spectrum obtained by gating on transitions above and below that state, as shown in Fig. 5(h).

Regarding spin assignments, the angular distribution given in Table II for the 431.5 keV transition connecting that isomer to the 17^{-} member of the 15^{-} band is consistent with a stretched dipole, suggesting spin and parity $18^{\pm}$. The fact that the 432 keV transition in Figs. 9(a) and 9(b) is more intense than the 388 keV γ ray, which is assigned as the $18^{-}\rightarrow 17^{-}$ member of the 15^{-} band, could be an argument for higher spin than $18\hbar$ for the 2588 keV state. (The short lifetime precludes multipolarities higher than quadrupole and of those, the $M2$ alternative can also be eliminated.) However, the higher population could also be explained by the favored path feeding through the next band (at 2900 keV) which becomes yrast. The suggested spin of $18^{(+)}$ implies $E1$ character for the 431.5 keV transition. The alternative of 18^{-} is less favored given the absence of a possible $E2$ branch to the 16^{-} state of the 15^{-} band.

The spectrum of transitions which precede the 2588 keV isomer [Fig. 9(c)] shows mainly a 312 keV transition which has been placed as a transition from another intrinsic (but short-lived) state at 2900 keV, and the first two members of each of the bands. The anisotropy of the 312 keV γ ray suggests stretched dipole character and the absence of a measurable lifetime (implying a limit of $\leqslant$ 8 ns) is consistent with $E1$ or $M1$ multipolarity and spin and parity of $19^{\pm}$.

These assignments are also consistent with the relative populations and the likely spin input in the reaction. A number of weakly populated nonyrast states with decays to the 9^{-} band are shown on the left of Fig. 3, including two suggested intrinsic states at 1597 and 1941 keV, also with some (limited) band structure.

C. Structures associated with the 1^{+} ground state and its band

Figure 4 shows part III of the level scheme involving decays to the ground-state band.

1. 0^{-} band

A relatively strongly populated sequence feeds a 27 ns isomer which decays by a 107.8 keV transition, as shown on the right-hand side of Fig. 4. No subsequent transitions are observed hence it has been placed on the 1^{+} ground state. The rapid change in conversion coefficient with energy and multipolarity, which is a help in assignment, but also a severe hindrance to the observation of low-energy transitions, is apparent in Fig. 10(a) which shows a combination of gates on cascade transitions in that band. The theoretical conversion coefficients for $M1$ transitions are 2.2, 4.3, 7.5, 2.96, and 10.5 for energies of 128, 102, 84, 64, and 41 keV, consistent with the drop in γ-ray intensities observed in that spectrum. Conversion for the 64 keV transition is less because it falls below the K edge, and the high γ-ray intensity of the 108 keV transition implies low conversion and defines it therefore as $E1$. The dominance of cascade $M1$ transitions over the crossover $E2$ transitions is a feature discussed later in the configuration assignment.

The 40.6 keV transition, which is the lowest energy transition clearly observed in this band, is close to the base of the sequence, as will be discussed below. Although we cannot discount the possibility that we have missed other very low-energy cascade transitions or crossover transitions ($E2$ conversion especially becomes very large), the population of the band would not be consistent with anything but a marginal increase in spin. The suggested spin and parity of 0^{-} is consistent with that argument, with the absence of any

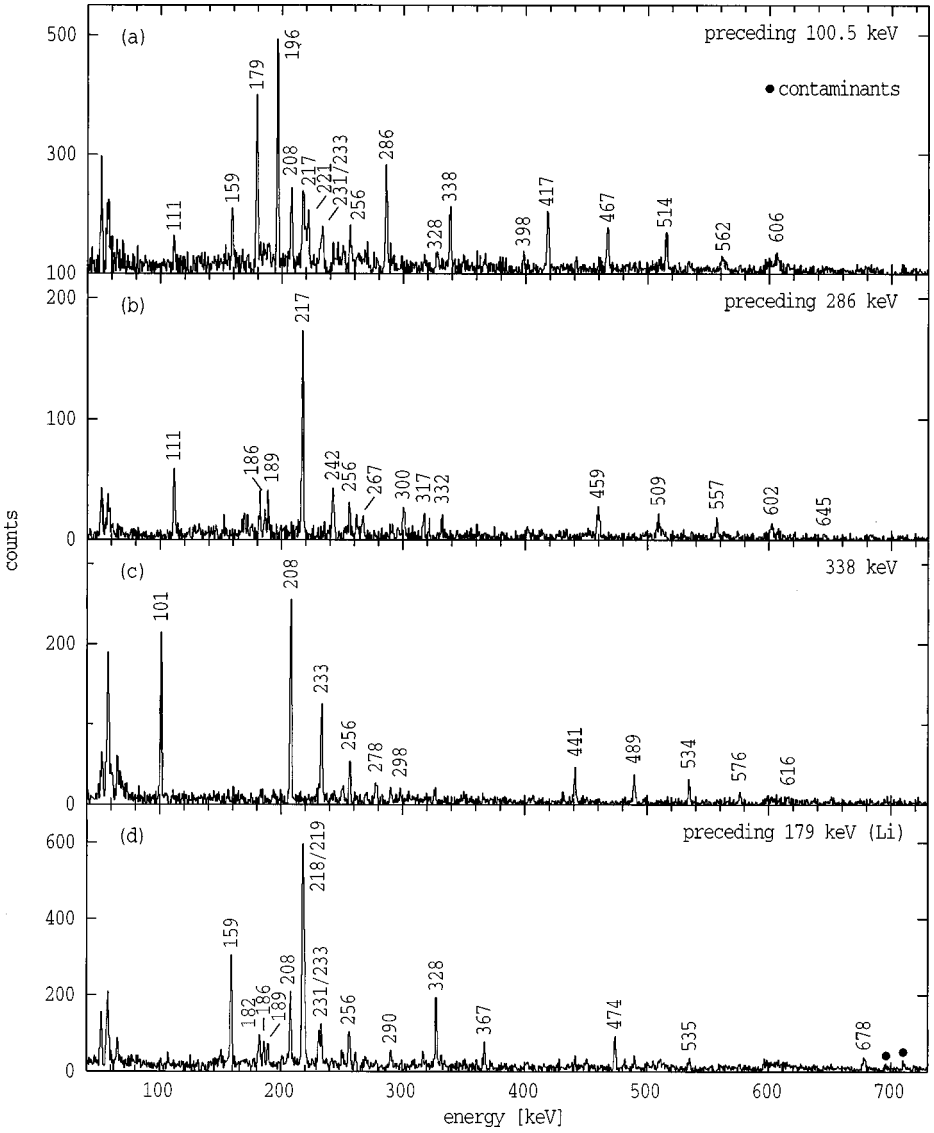

FIG. 6. Time correlated γ-γ spectra. (a) γ rays preceding the 100.7 keV transition which depopulates the 176 keV, 101 ns isomer. (b) γ rays preceding the 286 keV transition. (c) γ rays in prompt coincidence with the 338 keV transition. (d) γ rays preceding the 179 keV transition.

branch ($M2$) to the 2^+ state at 39.6 keV, and also with the perturbed structure which will be discussed later. The 108 keV transition is essentially isotropic, as expected for spin zero.

Feeding from states through the 252.5, 315.8, and 373.5 keV γ rays, none of which show measurable lifetimes, occurs into the bandhead and slightly above. These states are relatively more strongly populated in the ^{7}Li induced reaction, consistent with being nonyrast, and they are tentatively placed in a (1^-) band. The feeding via these transitions is part of the argument for the placement of an unobserved 23 keV cascade transition and a 63.2 keV $2^-\rightarrow 0^-$ crossover transition at the base of the 0^- band, although there are inherent difficulties in reaching this solution because that energy difference also corresponds to that of the strong 3^- to 2^- cascade transition.

The lifetime of 27 ns is obtained for the 0^- state from the analysis of a number of intermediate time spectra including those with gates on transitions within the band observed in the HpGe detectors, and with the 108 keV depopulating transition observed in the LEPS detector as shown in Figs. 5(f) and 5(g). In comparison, no lifetime is apparent [Fig. 5(e)] when the 102 keV in-band transition is substituted as ''stop.''

2. 1^+ band

A 39.5 keV transition which is placed as the first member of the 1^+ ground-state band is clearly resolved in the LEPS detectors (and partially resolved in the Ge detectors) from the 40.6 keV transition at the base of the 0^- band. Spectra obtained in the ^{7}Li bombardment, projecting the LEPS detector with gates on the 108 keV transition depopulating the 0^- band and a 409 keV transition which feeds the 3^+ state of the ground-state band, are compared in Fig. 11. The latter spectrum isolates the 71.4 and 39.6 keV cascade transitions in the 1^+ band which, from other coincidence spectra, is identified up to about spin 12.

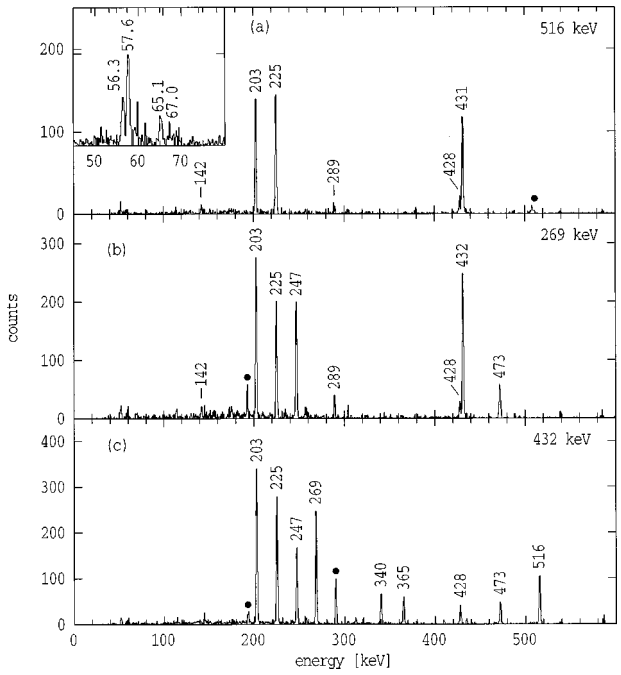

FIG. 7. γ-ray coincidence spectra gated on the 516, 269, and 432 keV transitions, in the out-of-beam region in the ^{11}B-induced reaction. Note that the relative γ-γ-time condition of ± 10 ns (used in this analysis only) reduces the efficiency at low energy. The inset shows the x-ray region as observed in the LEPS detector combining the same γ-ray gates.

3. Intrinsic states at 520 and 592 keV; $4^{(-)}$, (5^-) bands

The 409 keV transition mentioned above is delayed, establishing another isomer at 520 keV. It has several branches to higher members of the 1^+ band as shown in Fig. 4 and from these decays its spin and parities can be restricted to $4^\pm$ or 5^+. Spin 4 is favored by the anisotropy of the 409 keV transition. Positive parity, however, is unlikely, given the absence of a branch ($E2$) to the 2^+ state.

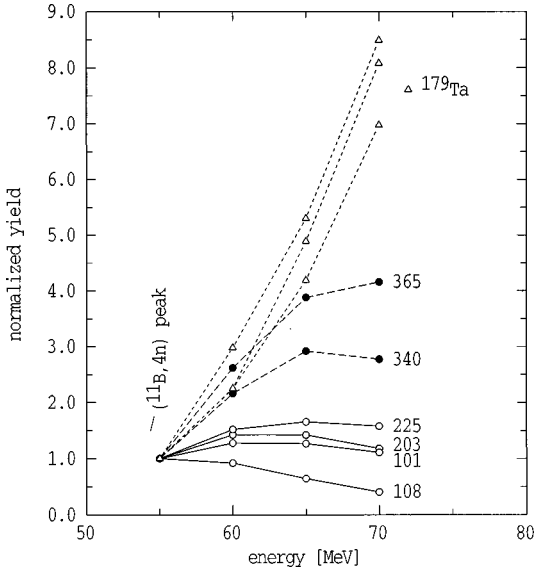

FIG. 8. Relative excitation functions, normalized to unity at 55 MeV, for selected γ rays observed in coincidence with α particles in the ^{11}B bombardments.

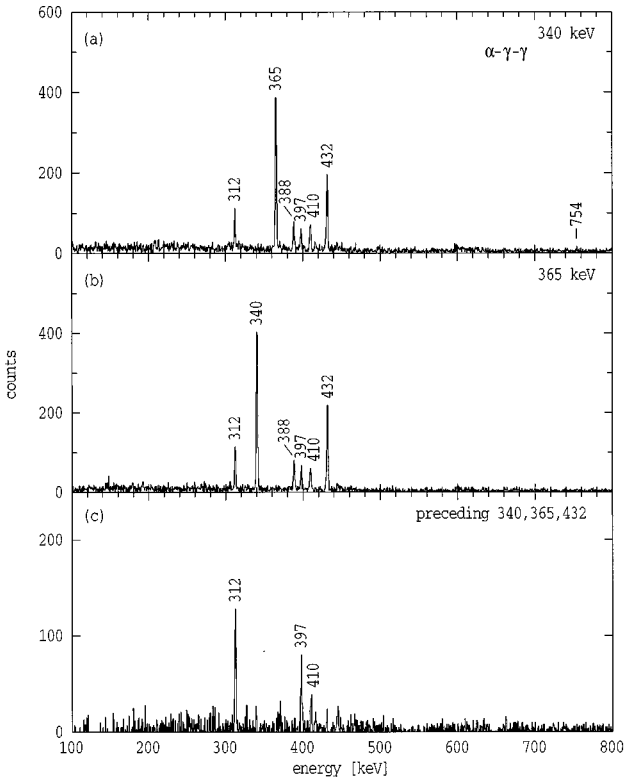

FIG. 9. Time-correlated coincidence spectra obtained in coincidence with α-particles in the ^{11}B bombardment and placed above the 15^- isomer. (a) Prompt coincidences with the 365 keV transition. (b) Prompt coincidences with the 340 keV transition. (c) Transitions which precede the decay of the $18^{(+)}$ isomer.

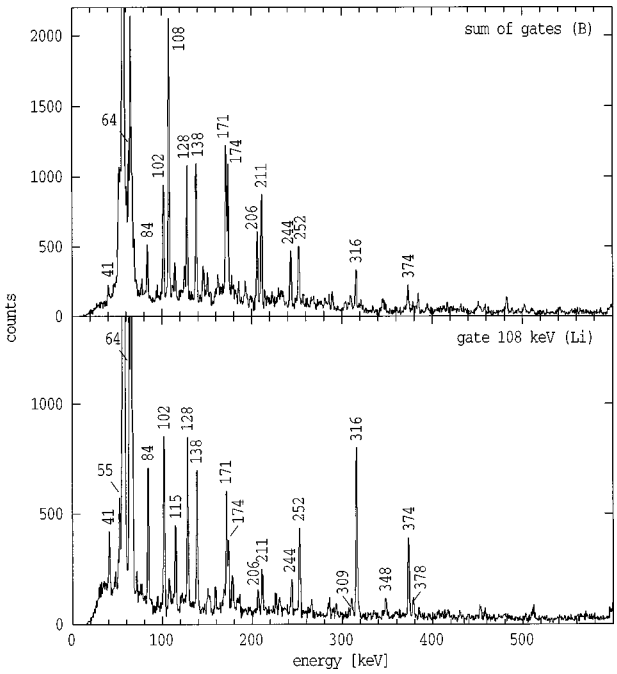

FIG. 10. Coincidence spectra associated with the 0^- band showing a combination of gates (on the 108, 128, 138, 171, and 174 keV transitions) in the ^{11}B bombardment (upper panel) and gated on the 108 keV transition in the ^{7}Li-induced reaction (lower panel), as measured in the Ge detectors.

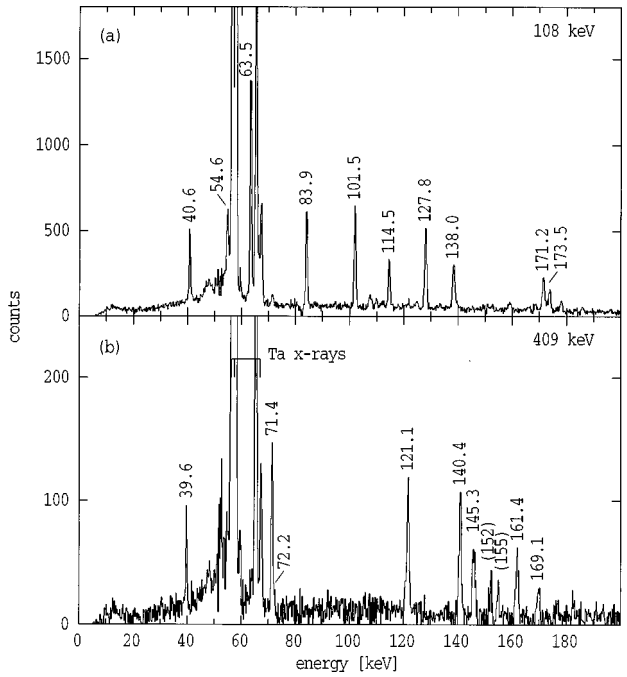

FIG. 11. Coincidence γ-ray spectra obtained in the LEPS detector with gates (a) on the 108 keV transition which depopulates the 0^- band, from data obtained in the ^{7}Li-induced reaction, (b) on the 409 keV transition which feeds the 1^+ band.

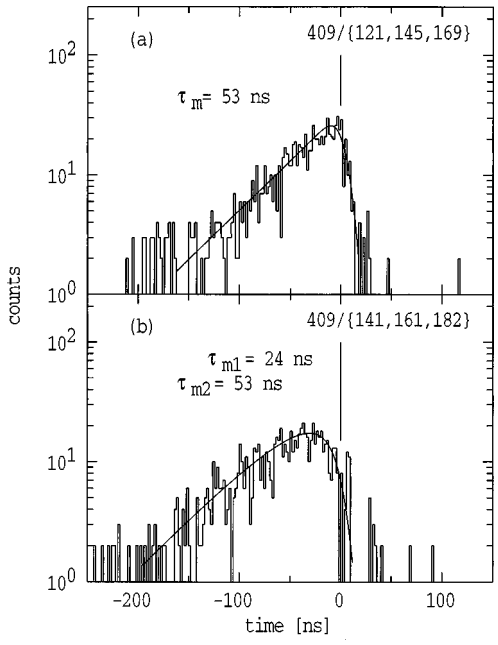

FIG. 12. Intermediate γ-γ-time spectra with gates on the 409 keV transition as start and on transitions in each of the two bands which feed it, observed in the LEPS detector.

Transitions feeding the 409 keV transition are evident in Fig. 11. These transitions, confirmed in both ^{7}Li and ^{11}B induced measurements, form into at least two rotational bands, which are not connected except at the bandhead. (Several other transitions in this spectrum are not firmly placed.) The presence of two intrinsic states, as inferred by the presence of two bands, is supported by the lifetime information extracted from the γ-γ-time spectra obtained by gating on transitions in each of the bands and the 409 keV transition. The corresponding spectra from the ^{7}Li induced measurement are shown in Fig. 12. Also shown are lifetime curves calculated with a single isomer to fit the spectrum obtained when gating on the band beginning with the 121 keV transition, Fig. 12(a), and with a sequence of two isomers, Fig. 12(b), when the gate is on the band beginning with the 140 keV transition. That analysis also implies that the latter band is higher. (Similar results were obtained in the ^{11}B-induced measurement.)

The only candidate we have for a transition connecting the two isomers is the 72.2 keV γ-ray indicated tentatively in the level scheme. From its low intensity [see Fig. 11(b)] and the associated intensity balance, it must have a conversion coefficient of $\sim$10 and therefore cannot be a pure $M1$ transition, but must have a substantial $E2$ admixture. This leads to a suggested assignment of $K^\pi=(5^-)$ or (6^-) for the 592 keV state. The lower of the spin possibilities for the 592 keV state has been marginally preferred because of the similarity in population of both bands.

D. Comparison with states assigned from particle-transfer and other studies

Many of the states assigned here have counterparts in the states observed in other reactions, as contained in the most recent compilation [17]. For example, the 2^+, 3^+, 4^+, and 5^+ states of the 1^+ band identified at 39.6, 111.0, 185.5, and 312.0 keV agree with the energies of 42(2), 111(2), 187(2), and 309(2) given in the compilation. A similar level of agreement is found for the 8^+, 9^+, and 10^+ states of the 8^+ band based at 176 keV and for the 10^- state of the 9^- band. The 107.8 keV 0^- state does not have a counterpart in the particle reactions but the 3^-, 4^-, and 5^- band members at 234.1, 318.1, and 419.6 keV agree with the (3^-), (4^-), and (5^-) states proposed at 231(2), 320, and 426 keV, the last two without specified errors. (Note, incidentally that this match would not have occurred without insertion of the 23 keV transition at the base of the 0^- band, as required by the coincidence data.) However, the compilation also lists a state at 414(2) keV, without a spin assignment and presumably one of these [the 414(2) or 426 keV state] should be associated with the (1^-) state we have placed at 423.6 keV. Continuing with states in Fig. 4, of the 520 keV 4^- and the 592 keV (5^-) bandheads, only the former has a partner in a 515(3) keV state (without spin assigned) in the compilation. Other states in part I of the scheme include the 461.7 7^- and 679 8^- states of our assigned 7^- band which agree with the 465(3) and 671(6) keV states of the same spin and parity in the compilation.

The compilers, Browne *et al.* [17], list a 6^- intrinsic state at 571(2) keV which coincides with our 573 keV (6^-) state although the existence of an (8^+) state at 574 keV could complicate the reaction studies because of the presence of several unresolved states. The only notable absence in the present scheme is a partner for the 258(2) keV state listed in the compilation and observed only in the ^{181}Ta(γ,n) reaction.

From the point of view of extra intrinsic states, while the (7^+) intrinsic state we have at 355 keV does not have a firm assignment in the compilations, a 361 keV (7^+) state was observed in proton transfer reactions on ^{179}Hf [20], a reac-

tion which should populate states related to the $9/2^+[624]$ ground state of ^{179}Hf. Adjustment of the approximate energies obtained in that study so that the energy of 75 keV 9^- state is matched would also place their observed (361 keV) state at about 355 keV. In fact, Warde *et al.* [20] made a firm assignment of this state as the $9/2^+[624]\otimes 5/2^+[402]$, 7^+ bandhead, on several bases, including the observation of $l=2$ transfer.

IV. MULTIQUASIPARTICLE CALCULATIONS

Calculation of the expected multiquasiparticle spectrum was carried out using the approach outlined in our recent publications (see, for example, Ref. [11]). The procedure involves a choice of single-particle levels and the pairing strength, and in order to avoid the limitations which cause collapse of the BCS solutions in regions of low and nonuniform level densities, the use of the Lipkin-Nogami formulation for calculation of the pairing.

The calculations use the prescription given by Nazarewicz *et al.* [21] to treat the Fermi level and pairing gaps self-consistently, to include particle-number conservation, and to have blocked states removed for multiquasiparticle configurations. For these calculations a space of 3 oscillator shells giving 64 levels (128 states) with about 34 active particles was used, taken initially from the Nilsson scheme. The results are sensitive to the choice of neutron single-particle levels in this case (more so than for our calculations in the lighter isotopes) because of the proximity to the $N=108$ subshell and because some of the energies change rapidly in this region, and therefore are difficult to define experimentally. Small deformation changes (including hexadecapole) affect, for example, the ordering of the $7/2^-[503]$ and $7/2^-[514]$ particle and hole states which compete in a number of the yrast configurations.

The calculated deformations for ^{180}Ta lie between those for ^{179}Hf and ^{181}W [22] and values of $\epsilon_2=0.237$ and $\epsilon_4=0.056$ have been used to give the initial set of single-particle states. Subsequently, the single-particle neutron energies for levels close to the Fermi surface used in the calculations were adjusted to reproduce approximately the average of the observed ^{179}Hf and ^{181}W one-quasineutron levels. The calculated deformations of ^{180}Ta and ^{181}Ta are very similar, hence the experimental one-quasiproton spectrum from ^{181}Ta was used to adjust the theoretical single-proton levels near the Fermi surface.

Note that we have neither corrected the one-quasiparticle energies for the rotational contribution to the bandhead energy, a correction of the order of $(\hbar^2/2\mathfrak{I})K$, nor added it to the predicted energies. This may introduce a mismatch in comparing states with $K=\Omega_n+\Omega_p$ in which that contribution is included to the extent that the multiquasiparticle energies are a linear sum of the one-quasiparticle energies, and those with $K=\Omega_n-\Omega_p$ in which the contribution tends to zero. If the $\Omega_n-\Omega_p$ state is correctly predicted, the energy of the $\Omega_n+\Omega_p$ state may be underestimated, as occurs occasionally in the following comparisons.

The two-quasiparticle states with $K^{\pm}=|\Omega_n\pm\Omega_p|$ predicted to be lowest are listed in Table V while the predicted four- and six-quasiparticle states (only those with the maximum coupling $K=\Omega_n+\Omega_p$), are given in Table VI. For completeness the most favored high-K states predicted are also included even though they are out of reach of this experiment.

The residual interactions which play an important role in determining the lowest states are also given in the table. These are calculated using the generalized form given by Jain *et al.* [23] for summing the two-quasiparticle contributions for each combination using the observed Gallagher-Moszkowski energies. The values listed differ slightly in some cases from those which would follow from the compilation of Ref. [23] because of a reevaluation of some of the empirical values. They follow the expectations for proton-neutron spin-spin interactions which favor $K=\Omega_n+\Omega_p$ for parallel intrinsic spins and $K=\Omega_n-\Omega_p$ if antiparallel. The final calculated state energies have been shifted (increased by 65 keV) so that the 1^+ state falls at 0 keV, after addition of the attractive residual interaction.

Note, however, that addition of the residual interactions deduced predominantly from the empirical values for two-quasiparticle cases is more approximate for the multiquasiparticle states since account is not taken of the possible redistribution of particle and hole amplitudes in estimating the higher seniority cases. A more complete treatment would require the interaction to include explicitly the dependence on occupation probabilities, as given, for example, for two-quasiparticle cases, by Massman *et al.* [24]. These would need to be generalized to the multiparticle case to use blocked wave functions calculated self-consistently for each configuration.

V. DISCUSSION

The distribution of the 70 calculated two-quasiparticle states with K from zero to 9, that can be formed from the superposition of the low-lying neutron and proton orbitals is shown in Fig. 14. Each neutron-proton pair gives rise to a doublet with $K^{\pm}=|\Omega_n\pm\Omega_p|$ with the triplet state (parallel Σ_n and Σ_p) lying lower in energy according to the Gallagher-Moszkowski rule.

A selection of the calculated states is listed in Table V together with the residual interactions and the suggested associations with observed states, to be discussed below. The main difficulties arise in identifying related states with intermediate-K values, of which there are a relatively large number expected in the same energy region (Fig. 13). As hinted at earlier, the experimental problem is that such states (nonyrast with $K\leqslant 6$) are populated, some even strongly in the ^{7}Li-induced reaction, but higher states in their bands are not, making their characterization difficult.

A. Configuration assignments, alignments, and magnetic properties

Table VII lists theoretical g_K values for selected configurations which will be discussed below. Experimental values of g_K-g_R for most of the bands as deduced from the observed γ-ray branching ratios are listed in Table II. Note that in some cases of ambiguous spin assignments, several possibilities are listed since the results depend both on the assumed spins and values of K.

Aligned angular momenta derived from the experimental data using a common reference for all bands are shown in

TABLE V. Selected two-quasiparticle states in ^{180}Ta.

K^{π}_{-}	K^{π}_{+}	Configuration [a]		E_{qp}	E^{res}_{+}	E_{calc} [b]		E_{expt}	
		ν	π			(-)	(+)	(-)	(+)
0^-	9^-	$9/2^+$	$9/2^-$	7	-71	143	-6	108	75
1^+	8^+	$9/2^+$	$7/2^+$	0	+65	**(0)**	130	0	176
2^+	7^+	$9/2^+$	$5/2^+$	357	-104	526	318		355
4^+	5^+	$9/2^+$	$1/2^+$	554	+70	549	689		
4^-	5^-	$9/2^+$	$1/2^-$	643	+36	672	744		
1^+	8^+	$7/2^-$	$9/2^-$	318	+50	333	433		(574)
0^-	7^-	$7/2^-$	$7/2^+$	311	-128	504	248		462
1^-	6^-	$7/2^-$	$5/2^+$	668	+59	674	792		683
3^-	4^-	$7/2^-$	$1/2^+$	865	-60	990	870		
3^+	4^+	$7/2^-$	$1/2^-$	954	-75	1094	944		
1^+	8^+	$7/2^{-\prime}$	$9/2^-$	776	-107	948	734		514
0^-	7^-	$7/2^{-\prime}$	$7/2^+$	769	+62	772	896		
1^-	6^-	$7/2^{-\prime}$	$5/2^+$	668	-97	830	636		(683)
3^-	4^-	$7/2^{-\prime}$	$1/2^+$	865	+81	849	1011		
2^+	7^+	$5/2^-$	$9/2^-$	449	-84	598	430		(355)
1^-	6^-	$5/2^-$	$7/2^+$	442	+56	451	563		(573)
0^-	5^-	$5/2^-$	$5/2^+$	799	-68	932	796		
4^+	5^+	$1/2^-$	$9/2^-$	514	+76	496	655		
3^-	4^-	$1/2^-$	$7/2^+$	508	-39	612	534		519
2^-	3^-	$1/2^-$	$5/2^+$	865	+48	882	978		
4^+	5^+	$1/2^{-\prime}$	$9/2^-$	471	-72	608	464		
3^-	4^-	$1/2^{-\prime}$	$7/2^+$	465	+51	479	581		
2^-	3^-	$1/2^{-\prime}$	$5/2^+$	821	-55	941	831		
3^+	6^+	$3/2^-$	$9/2^-$	710	+77	698	852		
2^-	5^-	$3/2^-$	$7/2^+$	704	-52	821	717		(592)

[a]Configurations. (π) $9/2^-$:$9/2^-[514]$; $7/2^+$:$7/2^+[404]$; $5/2^+$:$5/2^+[402]$; $1/2^+$:$1/2^+[411]$; **1/2$^-$**:$1/2^-[541]$. (ν) $1/2^-$:$1/2^-[521]$; **9/2$^+$**:$9/2^+[624]$; $5/2^-$:$5/2^-[512]$; $7/2^-_1$:$7/2^-[514]$; $7/2^-_2$:$7/2^-[503]$; $1/2^{-\prime}$:$1/2^-[510]$; $3/2^-$:$3/2^-[512]$.

[b]All shifted by +65 keV to match ground state.

Fig. 14. These provide some signature of the configurations involved, through approximate additivity. For example, bands involving the $9/2^+[624]$ neutron should exhibit an alignment of 1.5–2 $\hbar$, while an additional amount of about $\sim 0.7\hbar$ would come from the $9/2^-[514]$ proton. In the final analysis, distinctions made on this basis are less effective than in the lighter isotopes because of the relatively low alignments.

1. Two-quasiparticle states

Confirmation of the association of the 9^- state at 75 keV with the $\nu 9/2^+[624]\otimes\pi 9/2^-[514]$ configuration was given in our earlier publication [13] where the in-band γ-ray branching ratios λ were used to deduce $(g_K\text{-}g_R)/Q_0$ values for comparison with the values expected from the Nilsson configurations, additivity, and the rotational model. The values in Table II provide independent confirmation.

For the theoretical estimates it is useful to extract a value of the rotational value g_R and an empirical value of g_K for the $9/2^+[624]$ neutron. Since the magnetic moment of the 9^- isomer has been measured independently (as $4.77(5)\mu_N$ [25] corresponding to a gyromagnetic ratio of 0.530(6)), it can be used in the formula

$$g = g_R + (g_K - g_R)\frac{K^2}{I(I+1)},$$

with the weighted mean of the values from Table II for the 9^- band of g_K-$g_R = 0.30(1)$, giving $g_R = 0.26(1)$. This value differs slightly from that given in our earlier publication [13] because at that stage we were unaware of the availability of the measured quadrupole moment of 6.79(3) e b [26]. Using that value of g_R for the 9^- band and assuming the theoretical value of +1.28 for the $9/2^-[514]$ component, allows the extraction of an empirical value of $g_K(9/2^+[624]) = -0.15(2)$, not far from the expected Nilsson value of -0.20.

Antiparallel coupling of the $9/2^+[624]$ and $9/2^-[514]$ orbitals should give rise to a $K^\pi = 0^-$ band which we have associated with the structure built on the 107.8 keV state. As will be discussed in a following section, such a structure would not be regular, with some separation of even and odd-spin members.

As well as its perturbed character, a striking feature of the 0^- band is the dominance of cascade transitions, all cross-over ($E2$) transitions being weak, even at relatively high spins, as indicated by the branching ratios given in Table III.

TABLE VI. Selected four-, six-, and eight-quasiparticle states in ^{180}Ta.

K^π	Configuration [a]		E_{qp}	E_{res} (keV)	E_{calc}	E_{expt}
	ν	π				
12^+	$7/2^-9/2^+1/2^{-\prime}$	$7/2^+$	1564	−144	1420	
12^-	$5/2^-9/2^+1/2^{-\prime}$	$9/2^-$	1700	+258	1958	
13^+	$7/2^-9/2^+3/2^-$	$7/2^+$	1789	−170	1619	
13^-	$7/2^-9/2^+1/2^{-\prime}$	$9/2^-$	1570	−224	1346	1597
14^+	$7/2^-$	$7/2^+9/2^-5/2^+$	2004	−95	1909	1941
14^-	$7/2^-9/2^+3/2^-$	$9/2^-$	1796	0	1796	(1905)
15^+	$7/2^-9/2^+7/2^{-\prime}$	$7/2^+$	1859	−19	1840	
15^-	$9/2^+$	$7/2^+9/2^-5/2^+$	1693	−186	1507	1451
16^-	$7/2^-9/2^+7/2^{-\prime}$	$9/2^-$	1866	−146	1719	
18^+	$7/2^-9/2^+11/2^+$	$9/2^-$	2483	−150	2333	2588
19^-	$7/2^-9/2^+1/2^{-\prime}$	$7/2^+9/2^-5/2^+$	3257	−412	2845	2900
20^-	$7/2^-9/2^+3/2^-$	$7/2^+9/2^-5/2^+$	3483	−158	3225	
22^-	$7/2^-9/2^+7/2^{-\prime}$	$7/2^+9/2^-5/2^+$	3552	−364	3188	
24^+	$7/2^-9/2^+11/2^+$	$7/2^+9/2^-5/2^+$	4170	−395	3775	
26^-	$5/2^-9/2^+3/2^-7/2^-7/2^{-\prime}$	$7/2^+9/2^-5/2^+$	5406	−602	4804	
27^+	$5/2^-9/2^+11/2^+7/2^-1/2^{-\prime}$	$7/2^+9/2^-5/2^+$	5802	−64	5738	
28^+	$5/2^-9/2^+11/2^+7/2^-3/2^-$	$7/2^+9/2^-5/2^+$	6038	−448	5590	
30^+	$5/2^-9/2^+11/2^+7/2^-7/2^{-\prime}$	$7/2^+9/2^-5/2^+$	6108	−95	6013	

[a]Configurations. (π) $9/2^-$:$9/2^-[514]$; $7/2^+$:$7/2^+[404]$; $5/2^+$:$5/2^+[402]$; $1/2^+$:$1/2^+[411]$; **$1/2^-$**:$1/2^-[541]$. (ν):$1/2^-$:$1/2^-[521]$; **$9/2^+$**:$9/2^+[624]$; $5/2^-$:$5/2^-[512]$; $7/2^-$:$7/2^-[514]$; $7/2^{-\prime}$:$7/2^-[503]$; $1/2^{-\prime}$:$1/2^-[510]$; $3/2^-$:$3/2^-[512]$.

As will be shown below, this is a strong argument for the proposed assignment.

Kern and Struble [27] write the expression for the $M1$ transition in the odd-odd case as

$$B(M1;I_iK\rightarrow I_fK)=\frac{3}{4\pi}\mu_N^2(I_i1K0|I_fK)^2(G^{KK})^2,$$

where

$$G^{KK}=[\Omega_p(g_{\Omega_p}-g_R)+\Omega_n(g_{\Omega_n}-g_R)],$$

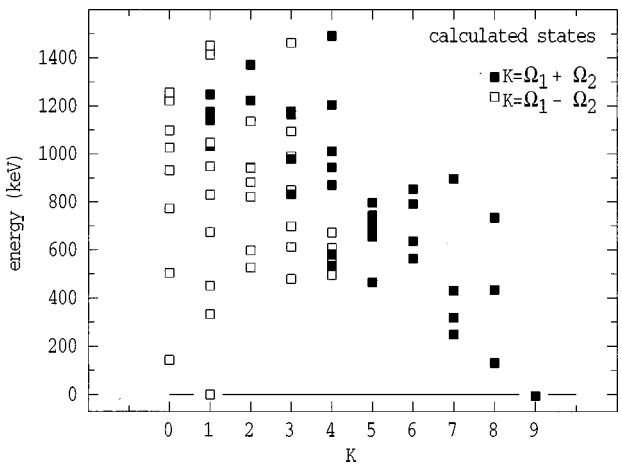

FIG. 13. Calculated two-quasiparticle states combining the lowest single-particle neutron and proton levels.

with the signs of Ω_p and Ω_n taken as in $K=\Omega_p+\Omega_n$.

For $K=0$ $G^{KK}=\Omega_p(g_{\Omega_p}-g_{\Omega_n})$, which is independent of g_R. For the present case with $\Omega=9/2$, $g_{\Omega_p}=1.28$ and $g_{\Omega_n}\sim-0.15$, $G^{KK}(0^-)=6.4$, compared to $G^{KK}(9^-)=2.7$ (with $g_R=+0.26$). Insertion of the value for $K=0$ in the expression above, leads to the favoring of cascade transitions observed. Note also that for $K=0$, cascade transitions will be pure $M1$ since the Clebsch-Gordan coefficients for the $E2$ component vanish.

The $B(E2)$ is given by

$$B(E2;I_iK\rightarrow I_fK)=\frac{5}{16\pi}(I_i2K0|I_fK)^2(eQ_0)^2$$

and the crossover-to-cascade γ-ray branching ratios λ then reduce to

$$\lambda=0.693\times\frac{5}{8}\times\frac{E_2^5}{E_1^3}\frac{(I-1)}{(2I-1)}\frac{(Q_0)^2}{(G^{KK})^2},$$

with the crossover and cascade energies E_2 and E_1 in MeV. The calculated values for the 0^- band agree reasonably well with the observed values as shown in Table III.

Of the other two-quasiparticle bands for which in-band branching ratios were obtained, the magnitude of g_K-g_R given in Table II for the band based on the 8^+176 keV state is in agreement with the value expected for the $\nu9/2^+[624]\otimes\pi7/2^+[404]$ configuration, the partner to the 1^+ ground state. However, the theoretical value is negative (-0.08),

TABLE VII. Values of g_K for selected two-, four-, and six-quasiparticle states.

K^π	Configuration [a]		g_K
	ν	π	
7^+	$9/2^+$	$5/2^+$	+0.46
7^+	$5/2^-$	$9/2^-$	+0.68
1^+	$9/2^+$	$7/2^+$	+3.4
8^+	$9/2^+$	$7/2^+$	+0.19
8^+	$7/2^-$	$9/2^-$	+0.84
8^+	$7/2^{-\prime}$	$9/2^-$	+0.56
7^-	$7/2^-$	$7/2^+$	+0.46
4^-	$1/2^-$	$7/2^+$	+0.71
4^-	$1/2^{-\prime}$	$7/2^+$	+0.33
4^+	$1/2^-$	$9/2^-$	+1.28
4^+	$9/2^+$	$1/2^+$	-0.04
5^+	$1/2^-$	$9/2^-$	+0.98
5^-	$3/2^-$	$7/2^+$	+0.61
12^+	$7/2^-9/2^+1/2^{-\prime}$	$7/2^+$	+0.13
12^-	$5/2^-9/2^+1/2^{-\prime}$	$9/2^-$	+0.27
13^+	$7/2^-9/2^+3/2^-$	$7/2^+$	+0.20
13^-	$7/2^-9/2^+1/2^{-\prime}$	$9/2^-$	+0.40
14^+	$7/2^-$	$7/2^+9/2^-5/2^+$	+0.92
14^-	$7/2^-9/2^+3/2^-$	$9/2^-$	+0.49
15^-	$9/2^+$	$7/2^+9/2^-5/2^+$	+0.73
18^+	$7/2^-9/2^+11/2^+$	$9/2^-$	+0.28
19^-	$7/2^-9/2^+1/2^{-\prime}$	$7/2^+9/2^-5/2^+$	+0.59
20^-	$7/2^-9/2^+3/2^-$	$7/2^+9/2^-5/2^+$	+0.65
22^-	$7/2^-9/2^+7/2^{-\prime}$	$7/2^+9/2^-5/2^+$	+0.43

[a]Configurations. (π) $9/2^-$:$9/2^-[514]$; $7/2^+$:$7/2^+[404]$; $5/2^+$:$5/2^+[402]$; $1/2^+$:$1/2^+[411]$; **$1/2^-$**:$1/2^-[541]$. (ν)$1/2^-$:$1/2^-[521]$; **$9/2^+$**:$9/2^+[624]$; $5/2^-$:$5/2^-[512]$; $7/2^-$:$7/2^-[514]$; $7/2^{-\prime}$:$7/2^-[503]$; $1/2^{-\prime}$:$1/2^-[510]$; $3/2^-$:$3/2^-[512]$.

which should result in dipole transitions with negative mixing ratios and therefore large negative A_2 values. The slightly positive value given in Table I for the 196.3 keV 9^+ to 8^+ transition implies a positive mixing ratio, implying in turn, a larger g_K value than expected. This could be evidence for mixing with the states of the $\nu 9/2^+[624]\otimes\pi 5/2^+[402]$ band which has a larger value of g_K.

Three possibilities are available for the character of the 8^+ 514 keV state and its associated band. These are

(i) $K=7$, $\nu 9/2^+[624]\otimes\pi 5/2^+[402]$,

(ii) $K=8$, $\nu 7/2^-[514]\otimes\pi 9/2^-[514]$,

(iii) $K=8$, $\nu 7/2^-[503]\otimes\pi 9/2^-[514]$.

Possibility (i) was discussed earlier in the context of identifying a band to be associated with the 355 keV 7^+ isomer. In this case the alignment [Fig. 14(b)] can be attributed to the $i_{13/2}$ neutron but the observed g_K-g_R value (Table II) is larger than the expected value of 0.20 (Table VII). It should be noted that this band would differ from the 8^+ band at 176 keV only by the exchange of the $5/2^+[402]$ and $7/2^+[404]$ protons. In ^{181}Ta the one-quasiparticle states are known (482 keV and the ground state) and have identical bands [28], but their closer proximity here means they are likely to mix, which would affect the observed g_K values. However, mixing with the 8^+ band should result in a smaller g_K value than expected, whereas the discrepancy is in the other direction.

Configuration (ii) is calculated to lie at a low energy ($\sim$433 keV) and the alignment observed [see Fig. 14(b)] could be roughly consistent with the contribution from the $9/2^-[514]$ proton. That contribution would be approximately given by the *difference* in alignment between the 8^+ (176 keV) band and the 9^- band. However, the measured g_K-g_R value is smaller than the expected value of 0.58.

Configuration (iii) also contains the $9/2^-[514]$ proton, hence the same alignment argument applies and in this case, the measured g_K-g_R values are in good agreement with the expected value of 0.30 deduced from Table VII. While this is the only one of the possibilities which gives the correct g_K-g_R value, the calculated energy given in Table V for this configuration is 220 keV higher than the observed state. This could imply that the $7/2^-[503]$ single-neutron energy used in the calculations is overestimated, a suggestion which is consistent with a comparable *underestimation* of the $7/2^-[514]$ energy deduced from the results for the 7^- band (discussed below) and which would in turn give rise to an artificially low energy (433 keV) for configuration (ii).

Returning to the other states, both the lack of alignment (FIg. 14) and the g_K-g_R values of the 7^- band at 462 keV agree with the $\nu 7/2^-[514]\otimes\pi 7/2^+[404]$ configuration. The

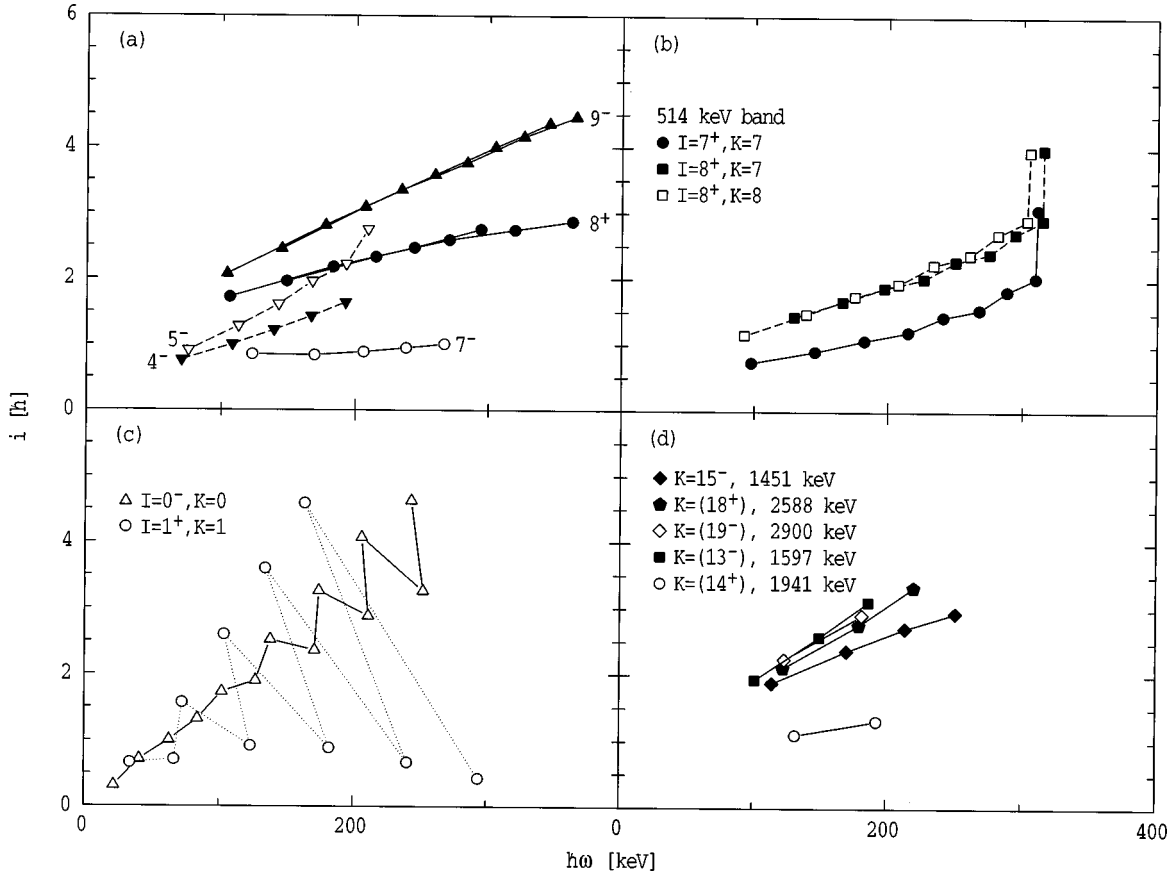

FIG. 14. Alignment curves for bands in ^{180}Ta as indicated. A common reference with parameters $\Im_0 = 31$ MeV$^{-1}\hbar^2$ and $\Im_1 = 70$ MeV$^{-3}\hbar^4$ has been subtracted.

energy of the 7^- configuration is underestimated by nearly 200 keV, suggesting an underestimation of the $\nu 7/2^-[514]$ energy in the single-particle spectrum.

Several states are calculated to be candidates for the intrinsic states at 520 and 592 keV but the former is possibly from the $1/2^-[521]\otimes 7/2^+[404]$ configuration which would have a g_K-g_R value of 0.41, in reasonable agreement with the observed value of ~ 0.49, which is sufficient to eliminate the alternative $1/2^-[510]\otimes 7/2^+[404]$ which would have g_K-$g_R = 0.03$, although it should be noted that the g_K value for the $\nu 1/2^-[510]$ orbital is sensitive to the deformation. The 592 keV state could then be from the $3/2^-[512]\otimes 7/2^+[404]$ configuration, in agreement again with the measured g_K-g_R value. Although its energy is calculated to be lower, the 5^+ state from the $1/2^-[521]\otimes 9/2^-[514]$ would have a much larger g_K-g_R than that observed.

Another alternative for the 520 keV state is the 4^+ $9/2^+[624]\otimes 1/2^+[411]$ configuration which would have g_K-$g_R = -0.31$. The magnitude would agree with experiment but the negative sign would lead to dipole transitions with negative A_2 values. The experimental values are not well determined because of contaminants, but on balance they do not favor this option, while the observed alignment [Fig. 14(a)] is ambiguous.

These arguments therefore favor the $1/2^-[521]\otimes 7/2^+[404]$ configuration discussed above, but lead to one other difficulty. From the results of the (d,t) reaction on the $7/2^+[404]$ ground state of ^{181}Ta, two strong peaks populated by $l=1$ transfer were identified with the 4^- and 3^- state from the same configuration, but at 712 and 785 keV, respectively [29]. The only resolution we can offer to the apparent conflict that arises if our suggested assignment is correct, is that the states observed in the (d,t) reaction are from the $1/2^-[510]\otimes 7/2^+[404]$ configuration. The $1/2^-[510]$ neutron orbital was not considered in the calculations of Ref. [29] but it is now known to be at a low energy as is the $1/2^-[512]$ orbital in both neighbouring odd neutron nuclei ^{179}Hf and ^{181}W and was considered in other studies [20].

2. Four- and six-quasiparticle states

15^- isomer. The argument was made in Ref. [13] that while the 15^- 45 μs isomer in ^{180}Ta had similarities to the 15^- isomer in ^{178}Ta (which has a much longer partial γ-ray half life of 101 ms [30,10]), the difference in decay strengths of the transition to the 9^- band was evidence of a difference in the 15^- configuration.

For a transition of multipole order λ, the reduced K-hindrance factor per degree of K forbiddenness f_ν, where $\nu = \Delta K - \lambda$, is defined as $f_\nu = (T^\gamma/T^W)^{1/\nu} = (f)^{1/\nu}$, where T^W is the Weisskopf single particle estimate and f is the corresponding hindrance factor. For the present interband transition, the degree of forbiddenness $\nu = 4$ and the lifetime in ^{178}Ta corresponds to an $E2$ hindrance, $f = 4.4\times 10^6$, and therefore a reduced hindrance of $f_\nu = 46$. While the shorter lifetime in ^{180}Ta arises partly because the $E2$ transition is higher in energy, the partial γ-ray lifetime for the 431.7 keV transition in ^{180}Ta corresponds to $f = 6.7\times 10^4$ and $f_\nu = 16$, much lower than in ^{178}Ta.

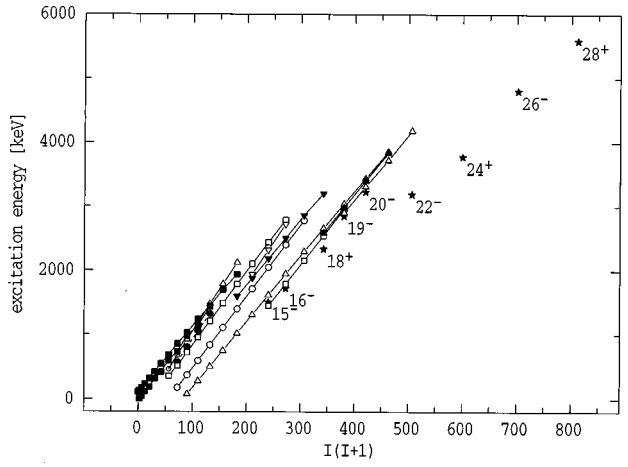

FIG. 15. Observed bands in ^{180}Ta compared to predicted yrast multiquasiparticle states, indicated by the stars.

In analogy with a correlation with similar differences in strengths in decays of the 6^+ isomers in the core hafnium isotopes (the 15^- states correspond to a coupling between the 6^+ configuration and the 9^- $\nu\pi$ state) the state in ^{178}Ta was suggested to be a mixture of the two alternative configurations

$$\nu^3 9/2^+[624]7/2^-[514]5/2^-[512]\otimes\pi 9/2^-[514]$$

and

$$\nu 9/2^+[624]\otimes\pi^3 9/2^-[514]7/2^+[404]5/2^+[402],$$

with the former (which we abbreviate to $\nu^3\pi$) dominant, whereas the state in ^{180}Ta was likely to be predominantly the latter ($\nu\pi^3$) configuration. That view is supported by the present multiquasiparticle calculations which confirm that the $\nu\pi^3$ alternative will be favored because of the change in the Fermi level, but more definitive evidence is provided by the properties of its rotational band now assigned. The dominance of the cascade transitions indicate a large g_K value and therefore mainly a proton configuration (see Table II for the quantitative analysis). This can be seen essentially from visual inspection of Fig. 9 where the crossover transitions are very weak—in complete contrast to the ^{178}Ta case where they are relatively intense (see Fig. 2 of Ref. [8]).

$18^{(+)}$ isomer and higher states. The calculations shown in Table VI and schematically in Fig. 15 also predict a relatively low-lying 18^+ state from a four-quasiparticle configuration, above which the six-quasiparticle states compete. The $\nu^3\pi$ structure of the calculated 18^+ state leads to a predicted g_K value of $+0.28$, in good agreement with the measured g_K-g_R of 0.05(3) (Table II). The cascade dipoles dominate in the 2900 keV (19^-) band, consistent with its suggested association with the six-quasiparticle state which is predicted at a similar energy and which would have a large predicted g_K of $+0.59$. Note the very large residual interaction (over 400 keV) which pushes that state close to the yrast line.

A 22^- six-quasiparticle state is also expected at about 3200 keV but has not been observed yet. While this is about the limit of the spin input, it could also be missed if it fell sufficiently low to be forced to decay via an $M3$ transition to the 19^- state at 2900 keV, resulting in a very long-lived isomer. Unfortunately a number of the transitions which would show evidence that such a state had been populated by exhibiting a long lifetime component, are already contaminated by long-lived components, the 431.5 keV transition by the 431.7 keV transition from the 45 μs isomer and the 365 and 340 keV transitions by activity lines.

One possible absence in the experimental spectrum is the predicted 16^- intrinsic state which would be likely to directly feed the 15^- isomer.

Also shown in Table VI are several eight-quasiparticle states, particularly the 26^- and 28^+ states which are depressed substantially by residual interactions. While out of reach of the present measurements, if they could be populated their decays would be likely to produce a cascade through the sequence of states both observed and predicted here.

A number of interconnected nonyrast states are shown on the left of Fig. 3, for example, those at 1338, 1579, 1597, 1905, and 1941 keV with likely spins in the range 11 to 14. Only fragmentary band structures are observed and a number of four quasiparticle are expected in this region, as listed in Table VI. Nevertheless, only one of those calculated states, the 14^+ state expected at about 1900 keV has a $\nu\pi^3$ structure. Such a configuration would lead to a dominance of cascade dipoles, as is observed for the band based on the 1941 keV state. This is the only one in the region which does not contain the $9/2^+[624]$ neutron, in agreement with the low aligned angular momentum [Fig. 14(d)] for the 1941 keV band. As well, although the calculated and observed energies are not as in good agreement as in the 14^+ case, the 1597 keV state has been associated with the 13^- state predicted at 1346 keV, consistent with its observed band alignment and observation of crossover transitions consistent (qualitatively) with a $\nu^3\pi$ structure.

B. Alignments and signature splitting

Two examples of $K=\Omega_n\pm\Omega_p$ partners are found in this work, the 1^+ and 8^+ states from the $\nu 9/2^+[624\uparrow]\otimes\pi 7/2^+[404\downarrow]$ configuration and the 0^- and 9^- states from the $\nu 9/2^+[624\uparrow]\otimes\pi 9/2^-[514\uparrow]$ configuration (with the intrinsic spin directions shown explicitly). The experimental signature splitting is evident in the alignment curves of Fig. 14 and is shown in the form of $(E_I-E_{I-1})/I$ against I^2 in Fig. 16. Even spins are favored in the 1^+ band. The splitting is much larger than that in the 0^- band and the splitting in the latter is also irregular near the bandhead, only developing favoring of the odd-spin states at higher spin.

It should be remembered that except for cases where *both* proton and neutron orbitals have $\Omega=1/2$, there is no diagonal contribution from Coriolis coupling equivalent to that which gives rise to signature splitting in odd-A nuclei. The shift between odd and even spin levels in $K=0$ bands in odd-odd nuclei is the so-called Newby splitting [31] which has been discussed in considerable detail, for example by Boisson, Piepenbring, and Ogle [32].

This spin-dependent part of the residual proton-neutron interaction gives an odd-even contribution in a rotational band equivalent to

$$[(-1)^{(I+1)}]\delta_{K,0}E_N\times P,$$

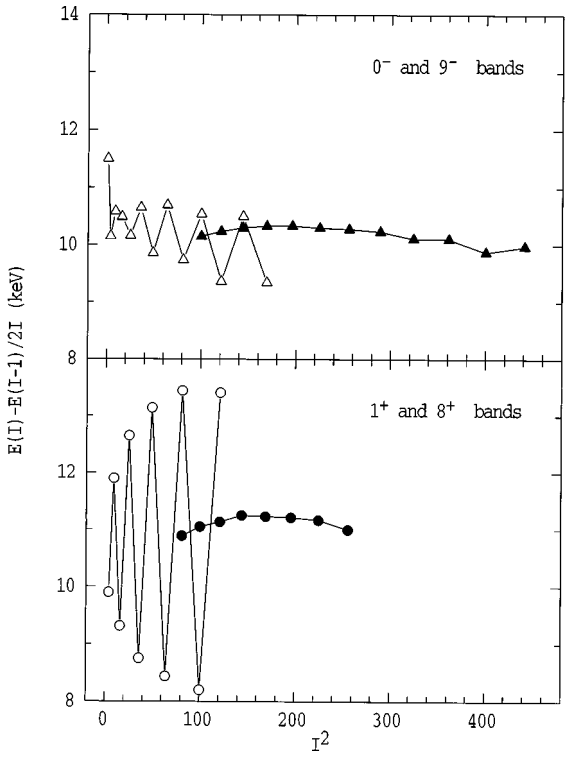

FIG. 16. Signature splitting observed in the 1^+ and 8^+ bands and the 0^- and 9^- bands.

where P is the parity and E_N is the Newby energy. (This follows the definition of Ref. [32].)

Unlike the Gallagher-Moszkowski terms which are attractive for $(\uparrow\uparrow)$ coupling and repulsive for $(\uparrow\downarrow)$ coupling, the Newby terms are described by both central and tensor terms in the residual interaction, and depend in detail on orbits and configurations. The role of the tensor component in the force has been emphasized recently [33].

The Newby splitting present in $K=0$ bands can be transferred to $K\neq 0$ bands by successive $(\Delta K=1)$ Coriolis coupling. This is exemplified in the present cases by the $K^\pi=1^+$ band whose rotational structure is perturbed mainly by the mixing between the bands obtained by combining the $7/2^+[404]$ orbital with the seven members of the $i_{13/2}$ neutron orbital leading to 14 bands ($|K|=\Omega_n\pm\Omega_p$) with significant Coriolis coupling between the neutron orbitals. The $K=0^+$ band based on the $7/2^+[633]\otimes 7/2^+[404]$ configuration is expected [32] to have $E_N\sim+40$ keV which leads indirectly to a favoring of even spin states in the observed 1^+ band with the related $9/2^+[624]\otimes 7/2^+[404]$ configuration. (Calculations which show how the perturbations are transferred to $K\neq 0$ bands, using simplified Coriolis mixing will be carried out elsewhere, using an approach similar to that used for two-neutron bands in the osmium isotopes [34].)

The expected Newby splitting in the unperturbed 0^- band from the $9/2^+[624]\otimes 9/2^-[514]$ combination was not calculated by Boisson, Piepenbring, and Ogle [32] but the value they give for the 0^- band from the related orbital pair $7/2^+[633]\otimes 7/2^-[523]$ is near zero (-0 keV is listed). The small value is due partly to a cancellation between a number of terms of different sign, hence it is not obvious what sign of splitting to expect. There is an experimental value (from ^{166}Ho) of ~ -32 keV and if a similar value were active, even spin states would be favored in the 0^- band. That could contradict the present assignment which has odd spins favored but as stated earlier, there is some uncertainty in the placement of transitions at the base of the band and the apparent spin favoring is irregular, pointing perhaps to more subtle mixing effects.

C. Candidates for intermediate states

As stated in the Introduction, a keen interest has been shown in the possibility of the presence of intermediate states which could be important for the understanding of the survival of ^{180}Ta in the stellar medium. The present study has not identified any states which have a clear path which would allow both excitation from the 9^- isomer and decay to the 1^+ ground state. This is indicated by the separation of the level scheme into distinct parts leaving part III (Fig. 4) with connections from the 1^+ ground state only to its band and to other low-K and intermediate-K states.

With respect to Coulomb excitation from the 9^- isomer [1], a state that has been identified here which may have some relevance is that at 1338 keV, possibly 11^-, whose main decay is the 1262 keV transition to the 9^- state, established through the path from the 1597 keV state. Another is the 1174 keV state shown in Fig. 3 as feeding the 10^- state of the 9^- band. We have not been able to establish with certainty a direct transition to the 9^- state (because of the absence of feeding transitions on which to gate) but both states are candidates for vibrational excitations based on the 9^- configuration. The energy of the 1174 keV state especially, is probably too low to be identified with predicted four-quasiparticle states. A 2^+ vibration based on the 9^- configuration would give two states with $K^\pi=11^-$ and 7^- (analogous to the $7/2^-[523]\otimes 2^+_\gamma$ states in ^{165}Ho which give rise to isospectral bands [35]). Several states, possibly 7^- are seen in this excitation energy region in Fig. 2, but in any case, strong population would be unlikely in the present reactions. Nevertheless, such a state (and its band members) would have the prospect of decaying through the intermediate spin states of the 1^+ band and possibly the 0^-, 4^-, and (5^-) bands identified in Fig. 4, although the last three all involve paths which proceed through isomers so that the absolute transition rates for excitation connecting through the 1^+ band are still small.

A final comment on the structure of the level scheme of ^{180}Ta is appropriate; a peculiarity of the level scheme which arises from position of the Fermi levels among particular Nilsson orbitals is the relatively large number of states of similar spin, occurring at relatively low excitation energies. One consequence is the presence of interconnecting $M1$ transitions as shown in Fig. 2. This situation is to be contrasted for example, with the level scheme of ^{178}Ta [12] which does not show that feature.

D. Concluding remarks

In summary, a comprehensive study has been carried out of ^{180}Ta utilizing a number of different techniques to isolate intrinsic states and their rotational bands, whose properties serve to characterize their configurations. The remaining un-

certainties in the scheme result from the very low energy of transitions which are necessarily involved in very low-K bands, and in this nucleus, the relatively high density of intermediate-K states whose associated bands cannot be populated over a large enough spin range to clearly identify their bands. Ambiguities also remain regarding assignments to several of the two-quasiparticle bands, particularly the 7^+ isomer at 355 keV, and possibly the $4^{(-)}$ isomer at 520 keV. At this stage, clear candidates for strong excitations which could connect the 1^+ ground state and the 9^- isomer have not been identified but a number of four- and six-quasiparticle states have been observed and characterized, and yrast six- and eight-quasiparticle states at slightly higher spins than currently accessible have been predicted.

ACKNOWLEDGEMENTS

We would like to thank the academic and technical staff of the ANU Heavy Ion facility for their continuing support in these studies.

[1] C. Schlegel, P. von Neumann-Cosel, F. Neumeyer, A. Richter, S. Strauch, J. de Boer, C.H. Dasso, and R.J. Peterson, Phys. Rev. C **50**, 2198 (1994).
[2] C.B. Collins, C.D. Ebehard, J.W. Glesener, and J.A. Anderson, Phys. Rev. C **37**, 2267 (1988).
[3] C.B. Collins *et al.*, Phys. Rev. C **42**, R1813 (1990).
[4] J.J. Carroll, C.B. Collins, P. von Neumann-Cosel, D.G. Richmond, A. Richter, T.W. Sinor, and K.N. Taylor, Phys. Rev. C **45**, 470 (1992).
[5] Zs. Németh, Phys. Rev. C **45**, 467 (1992).
[6] S.A. Karamian *et al.*, Z. Phys. A **356**, 23 (1996).
[7] M. Loewe *et al.*, Z. Phys. A **356**, 9 (1996).
[8] F.G. Kondev, G.D. Dracoulis, A.P. Byrne, M. Dasgupta, T. Kibédi, and G.J. Lane, Nucl. Phys. **A601**, 195 (1996).
[9] M. Dasgupta, P.M. Walker, G.D. Dracoulis, A.P. Byrne, P.H. Regan, T. Kibédi, G. Lane, and K.C. Yeung, Phys. Lett. B **328**, 16 (1994).
[10] F.G. Kondev, G.D. Dracoulis, A.P. Byrne, S. Bayer, and G.J. Lane, Phys. Rev. C **54**, R459 (1996).
[11] F.G. Kondev, G.D. Dracoulis, A.P. Byrne, T. Kibédi, and S. Bayer, Nucl. Phys. **A617**, 91 (1997).
[12] F.G. Kondev, G.D. Dracoulis, A.P. Byrne, and T. Kibédi, Nucl. Phys. **A632**, 473 (1998).
[13] G.D. Dracoulis, F.G. Kondev, A.P. Byrne, T. Kibédi, S. Bayer, P.M. Davidson, P.M. Walker, C. Purry, and C.J. Pearson, Phys. Rev. C **53**, 1205 (1996).
[14] F. Lidén, A. Johnson, A. Kerek, E. Dafni, and M. Sidi, Nucl. Instrum. Methods Phys. Res. A **273**, 240 (1988).
[15] T. Inamura, M. Ishihara, T. Fukuda, T. Shimoda, and H. Hiruta, Phys. Lett. **68B**, 51 (1977).
[16] D.R. Zolnowski, H. Yamada, S.E. Cala, A.C. Kahler, and T.T. Sugihara, Phys. Rev. Lett. **41**, 92 (1978).
[17] E. Browne, Nucl. Data Sheets **52**, 127 (1987); **71**, 81 (1994).
[18] S.E. Kellogg and E.B. Norman, Phys. Rev. C **31**, 1505 (1985).
[19] G.D. Dracoulis, A.P. Byrne, T. Kibédi, T.R. McGoram, and S.M. Mullins, J. Phys. G **23**, 1191 (1997).
[20] E. Warde, G.J. Costa, D. Magnac, R. Seltz, C. Gerardin, M. Buenerd, Ph. Martin, and C.A. Wiedner, Phys. Rev. C **27**, 98 (1983).
[21] W. Nazarewicz, M.A. Riley, and J.D. Garrett, Nucl. Phys. **A512**, 61 (1990).
[22] P. Moller, J.R. Nix, W.D. Myers, and W.J. Swiatecki, At. Data Nucl. Data Tables **59**, 185 (1995).
[23] Kirain Jain, O. Burglin, G.D. Dracoulis, B. Fabricius, N. Rowley, and P.M. Walker, Nucl. Phys. **A591**, 61 (1995).
[24] H. Massmann, J.O. Rasmussen, T.E. Ward, P.E. Haustein, and F.M. Bernthal, Phys. Rev. C **9**, 2312 (1974).
[25] B. Burghard *et al.*, Phys. Lett. **92B**, 64 (1980).
[26] M. Wakasugi, W.G. Jin, T.T. Inamura, T. Murayama, T. Wakui, H. Katsuragawa, T. Ariga, T. Ishizuka, and I. Sugai, Phys. Rev. A **50**, 4639 (1994).
[27] J. Kern and G.L. Struble, Nucl. Phys. **A286**, 371 (1977).
[28] G.D. Dracoulis, A.P. Byrne, S.M. Mullins, T. Kibédi, F.G. Kondev, and P.M. Davidson, this issue, Phys. Rev. C **58**, 1837 (1998).
[29] R.A. Dewberry and R.A. Naumann, Phys. Rev. C **28**, 2259 (1983).
[30] F. Dubbers, L. Funke, P. Kemnitz, K.D. Schilling, H. Strusny, E. Will, G. Winter, and M.K. Balodis, Nucl. Phys. **A315**, 317 (1979).
[31] N.D. Newby, Jr., Phys. Rev. **125**, 2063 (1962).
[32] J.P. Boisson, R. Piepenbring, and W. Ogle, Phys. Rep. **26**, 99 (1976).
[33] A. Covello, A. Gargano, and N. Itaco, Phys. Rev. C **56**, 3092 (1997).
[34] G.D. Dracoulis, C. Fahlander, and M.P. Fewell, Nucl. Phys. **A383**, 119 (1982).
[35] G. Gervais *et al.*, Nucl. Phys. **A624**, 257 (1997).